KLUGHERTZ, Guillaume
Promotion 2012
Année 2011-2012

Diplôme d'ingénieur TELECOM PHYSIQUE STRASBOURG

Mémoire de stage de 3ème année

« Simulated annealing study of the disordered quantum magnet $LiHo_xEr_yY_{1-x-y}F_4$ »

LQM-IPMC-EPFL
Station 3
1015 Lausanne
Suisse

Supervisor : Bastien Dalla Piazza
[+41 21 69] 34144
bastien.dallapiazza@epfl.ch

05/03/2012 - 20/07/2012

ACKNOWLEDGEMENTS

The master thesis presented here has been achieved within the Laboratory for Quantum Magnetism (LQM) at EPFL.
I wish to thank Henrik Rønnow, associate professor and head of the laboratory, for boosting my interest in magnetism and for giving me the opportunity to carry out my master thesis in his group.
I am also especially grateful to Bastien Dalla Piazza, for his useful and smart advices, and for all his support during this project.
Furthermore, I would like to thank Krunoslav Prša, Neda Nikseresht Ghanepour and Julian Piatek, for their human qualities and inspiring discussions, for their inventiveness and their numerous tips, and for the precious time they have given me sharing different scientific aspects.
I would like to thank Paul Freeman, Jonathan White, Arash Alahgholipour Omrani, Ivan Kovacevic and Diane Lançon for their companionship, their cheerfulness, and for every moment we shared.
Finally, my thesis work would not have been feasible if I hadn't found an accommodation opportunity in Lausanne, and I am infinitely thankful to Caroline Pletscher for helping me in this arduous task.

TABLE OF CONTENTS

RESUME

Etude du composé magnétique désordonné $LiHo_xEr_yY_{1-x-y}F_4$ par recuit simulé

Les transitions de phase quantique et classique de quelques composés ($LiErF_4$, $LiYbF_4$, $LiGdF_4$ and $LiTmF_4$) sont calculées à l'aide de la théorie de champ moyen. Ces calculs préliminaires ont permis de révéler l'existence d'une nouvelle phase antiferromagnétique dans $LiErF_4$ pour de forts champs magnétiques, ainsi qu'une brisure de symétrie inattendue dans $LiGdF_4$. Ils ne permettent néanmoins pas de retrouver les valeurs critiques des transitions de phase de $LiErF_4$ car les fluctuations sont négligées par cette théorie, et appellent donc à mener des simulations plus sophistiquées.

Nous présentons ensuite les preuves analytiques et numériques de la validité du modèle effectif $S_{eff} = \frac{1}{2}$ lorsqu'il est appliqué à la description de l'antiferroaimant dipolaire $LiErF_4$. Nous montrons que, à faible champ et basse température, cette approche implémentée dans des simulations en champs moyen permet de reproduire aussi bien qualitativement que quantitativement le comportement du composé $LiErF_4$, produisant des résultats très proches de ceux obtenus par les calculs en champ moyen dans l'espace de Hilbert complet. Elle nécessite toutefois d'être améliorée afin de pouvoir décrire correctement la physique de $LiHoF_4$.

Ce modèle réduit sert ensuite de base à des calculs de Monte Carlo classiques appliqués à $LiErF_4$, permettant de déterminer les quantités thermodynamiques du système ainsi que l'évolution les paramètres d'ordre en fonction de la température et du champ magnétique. Ces simulations produisent des résultats beaucoup plus proches des valeurs expérimentales que celles basées sur l'approximation de champ moyen. Bien que la température critique théorique soit encore surestimée de 34%, ce modèle effectif permet de retrouver les exposants critiques de la transition de phase classique de $LiErF_4$.

ABSTRACT

Simulated annealing study of the disordered quantum magnet $LiHo_xEr_yY_{1-x-y}F_4$

Thermal and quantum phase transitions of some rare earth compounds ($LiErF_4$, $LiYbF_4$, $LiGdF_4$ and $LiTmF_4$) are established using the mean field theory. These preliminary calculations allowed evidencing the existence of a novel high-field antiferromagnetic phase in $LiErF_4$, and a still unexplained symmetry breaking in $LiGdF_4$. But the discrepancies with experimental results impel a more sophisticated method.

We then present analytical and numerical evidence for the validity of an effective $S_{eff} = \frac{1}{2}$ approach to the description of the dipolar coupled antiferromagnet $LiErF_4$. We show that the $S_{eff} = \frac{1}{2}$ approach, when implemented in mean field calculations, is able to capture both the qualitative and quantitative aspects of the physics of $LiErF_4$ at small external field and low temperature, yielding results that agree with those obtained in the full Hilbert space using mean field theory. This model nevertheless still fails to describe the $LiHoF_4$ system and needs to be improved.

We finally use this toy model as a basis for classical Monte Carlo simulations of $LiErF_4$, which allows the calculation of thermodynamical quantities of the system, as well as the evolution of the order parameters as a function of field H and temperature T. These calculations yield results that are much closer to the experiments than those based on the mean field approximation. Although the theoretical critical temperature is still overestimated by 34%, the critical exponents computed from this effective model correspond to those found experimentally.

TABLE OF FIGURES

INTRODUCTION

The study of quantum phase transitions and especially the phenomena occurring in the vicinity of critical points has attracted great interest in recent years because it would allow a better understanding of many issues of condensed matter physics such as high-temperature superconductivity, metal-insulator or superconductor-insulator transition, or spin glasses transitions. The discovery in the early seventies of materials exhibiting no apparent long range magnetic ordering at low temperatures while being subject to a magnetic phase transition into a randomly frozen spin configuration [6], i.e. spin glasses, still challenges theorists. In 1946 Luttinger and Tisza [18] already discussed the possibility that magnetic ordering could arise only from the magnetic dipolar coupling and geometrical configuration of the atoms.

One of the main research topics of the LQM is the study of the dipolar coupled quantum magnet $LiREF_4$ compound where RE (for Rare Earth) may be holmium (Ho), erbium (Er), yttrium (Y) or a mixture. The mixture (Ho / Y) has the properties of a spin glass and the mixture (Ho / Er) may be a superposition of two types of spin glasses. The LQM has many very interesting experimental results which are fundamental for the quantum magnetism community.

From a theoretical point of view, these materials are very important because the microscopic model describing them is known very precisely: one can really write a Hamiltonian of spins (only degrees of freedom) including all the quantitative details. It is uncommon that theory and experiment can be compared with such accuracy.

One of the challenges is to describe the ground state of the system when dealing with a mixture, and thus a random distribution of different kinds of ions. Previous projects of LQM consisted of calculating a self-consistent mean field solution of a disordered arrangement of ions. When the system approaches a spin glass state, many metastable states appear and the system will "freeze" in a random state. The mean field approach is not good in this case: the system will effectively freeze but there is no way of knowing if this state has a physical sense or is an artifact. Some clues suggest that there is a spin-glass phase in $LiREF_4$ compounds, but the quantum magnetism community still lacks solid theoretical evidence. It seems obvious that a more sophisticated and realistic approach is essential for the LQM to clarify the gray areas of $LiREF_4$ compounds and to create new research paths.

The simulated annealing Monte Carlo technique is used to simulate more accurately the physical phenomena occurring when a material is slowly cooled down to let it find its ground state. It is suited to minimize a cost function (the free energy in this case) based on a very large number of parameters (e.g. the quantum state of each individual ion). The goal is to implement this technique and calculate key quantities - magnetization, susceptibility, structure factor, specific heat - and to compare with experimental results.

1. THE $LiREF_4$ COMPOUNDS

The lithium-[rare earth(s)]-tetrafluoride compounds are subject to a wide range of quantum phenomena. Their magnetic properties being well characterized, these insulators are found to be excellent models to compare quantitatively the experimental results with theory.

The magnetic moments are mainly affected by the crystal field anisotropy and magnetic dipole-dipole interaction, dominant over the exchange interactions because of the tightly bound *4f* electrons. $LiREF_4$ compounds crystallize in a tetragonal Scheelite-type structure which belongs to the $I4_1/a$ space group, and each unit cell contains four rare earth ions.

Further details on the various compounds are given in Appendix 1.

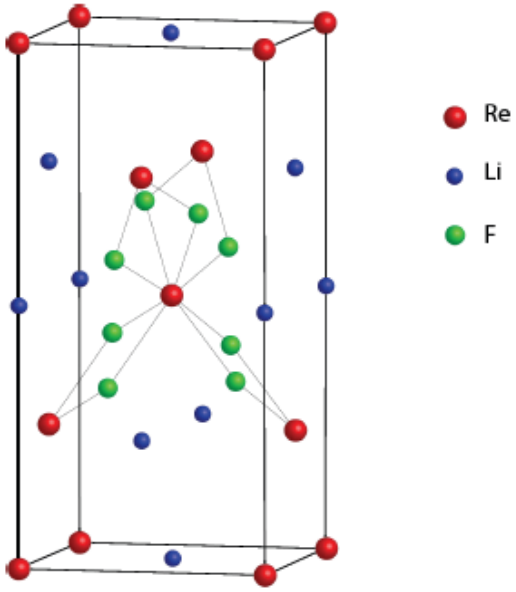

Figure 1 : $LiREF_4$ unit cell. For clarity reasons, only fluoride ions closest to the RE ion at (a/2, a/2, c/2) are represented.

$LiREF_4$ is an ideal system to study a variety of compounds because it crystallizes for almost all rare earths with little structural change, only the positions of the fluoride ions and lattice parameters are slightly modified.

Another huge advantage of $LiREF_4$ is the existence of a isostructural dilution series in which part of the RE ions are randomly replaced by nonmagnetic rare earths such as yttrium or lutetium, making these compounds suitable for the study of isolated dipoles, of dipoles interacting randomly or the highly correlated pure system,. All these compounds are transparent to light, electrical insulators, thermally stable and inert.

$LiYF_4$ doped with a small percentage of rare earths is widely used in laser technology because of the long lifetimes of the crystal field energy levels [29].

1.1. $LiHoF_4$

Most of the research has so far focused mainly on $LiHoF_4$ and its dilutions $LiHo_xY_{1-x}F_4$ which show a wide variety of phenomena, ranging from tunneling effects between moments or walls of magnetic domains, to studies of "quantum annealing", quantum entanglement or clusters of spins coherently oscillating [5, 4, 9, 8].

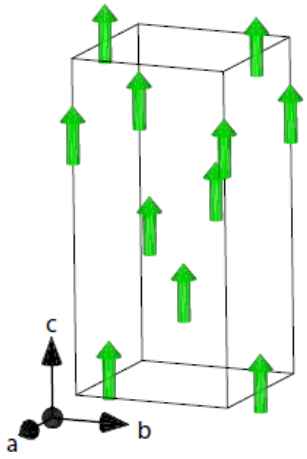

Figure 2 : Magnetic structure of the $LiHoF_4$ ferromagnet.

In $LiHo_xY_{1-x}F_4$, Ho^{3+} ions interact mainly via the magnetic dipolar interaction. The pure system is a physical realization of the famous Transverse Field Ising Model (TFIM) with a ferromagnetic phase below $T_c = 1.53K$ and a quantum critical point at $H_c = 5T$ [2]. When non-magnetic yttrium ions are substituted for the Ho ions, random frustrations appear. The crystal behaves differently depending on the proportion of Ho ions: it goes from a ferromagnetic state ($x = 1$) to a ferromagnetic state ordered by long range interactions with significant memory effects ($x = 0.44$), a spin-glass ($0.1 < x < 0.3$) and a liquid spins phase ($x < 0.1$), often called "antiglass state".
The consequences of crystal symmetry breaking due to dilution and memory effects on the appearance of magnetic ordering (cooling without external field leads to a ferromagnetic order, whereas with a transverse field appears a spin-glass) in $LiHoF_4$ still lack solid explanations. While theorists are still debating the various aspects of spin glasses, it is generally accepted that the random arrangement of ions introduced by the dilution through the dipolar coupling and the transverse field leads to frustration preventing the moments to develop a long range ordering.

Although the effective TFIM (restricted to the degenerate ground state doublet only) gives a good approximation of the real system, experiments of inelastic neutron scattering [22] and susceptibility measurements [2] have shown that the hyperfine interaction, although very weak, acts as a bath of nuclear spins (that is to say a reservoir of degrees of freedom), and has in fact a non-negligible influence on the phase diagram shape by translating the critical field to higher values, as well as that of the excitation

spectrum around the quantum phase transition, which was interpreted as the effects of quantum decoherence. It was also shown in these studies that the thermal fluctuations tend to decouple the electronic subsystems to the spin bath.

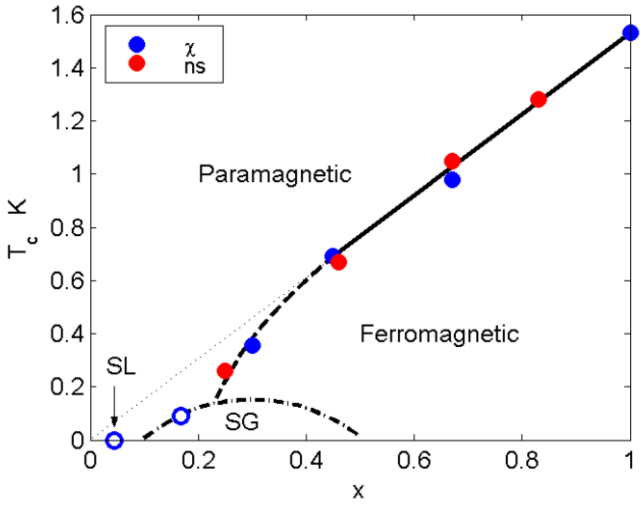

Figure 3 : Experimental phase diagram of $LiHo_xY_{1-x}F_4$ [21]. Blue points are susceptibility measurements, red ones are from neutron scattering experiments. For x=0.145, no freezing was observed, suggesting a spin liquid (SL).

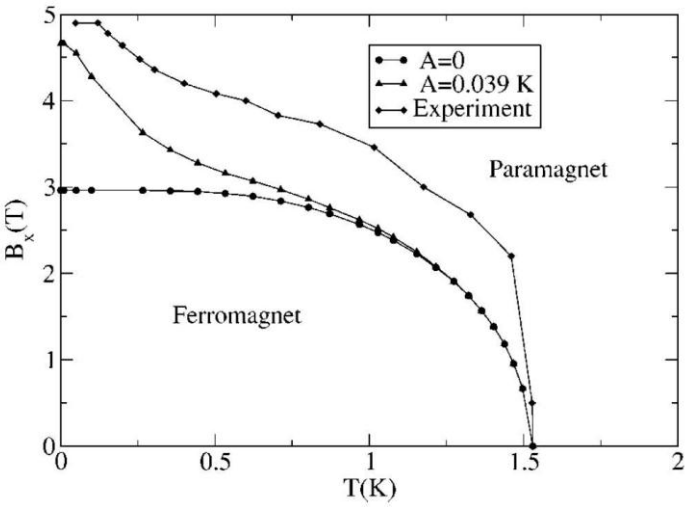

Figure 4 : H_x-T phase diagram of $LiHoF_4$ [7]. The experimental (above) is from Bitko *et al.* [2]. The middle one (triangles) is from a numerical simulation taking the hyperfine interaction into account, the bottom one neglecting it. *A* is the hyperfine factor.

The first excited state lying more than 10K above the ground state, $LiHoF_4$ can be considered as an almost perfect realization (neglecting the hyperfine interaction) of the Random Field Ising Model (or RFIM) [23], like the Edwards-Anderson model (short-range interactions) or the Sherrington and Kirkpatrick model (long range). The quantum nature of this system appears only in high transverse fields, of the order of the energy gap between the ground state and first excited state, where the quantum fluctuations induced by the transverse hyperfine interaction becomes significant. Finally, some experimental studies [21, 30] show a spin glass transition in $LiHo_{0.167}Y_{0.833}F_4$ while others [14], more recent, don't.

1.2. $LiErF_4$

Despite the many possible arrangements among the $LiREF_4$ materials, most of the work has focused on $LiHoF_4$ and its dilutions. The existence of ferromagnetic or antiferromagnetic states resulting only from the joint action of the dipolar interaction and the geometry of the structure has already been pointed out over 60 years ago by Luttinger and Tisza [18]. $LiErF_4$ is an example of the $LiREF_4$ series which exhibits an antiferromagnetic ordering below $T_N = 373mK$.
The experimental work of LQM make $LiErF_4$ the only purely dipolar antiferromagnet that has been studied in detail, allowing the characterization of all the parameters of the microscopic Hamiltonian.

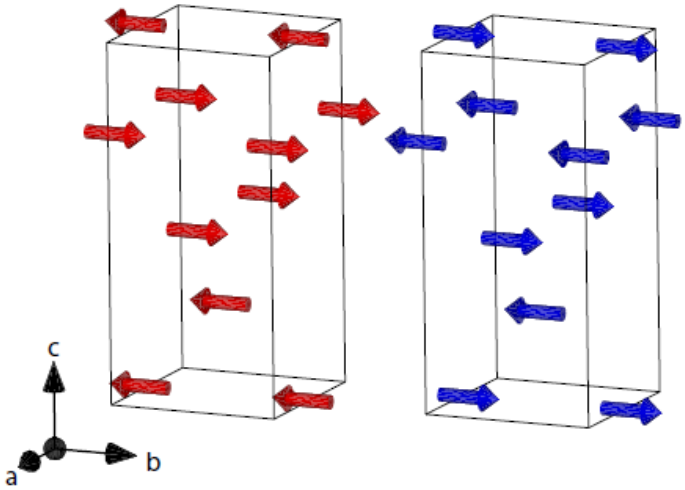

Figure 5 : Possible magnetic structures of $LiErF_4$: nearest neighbour antiferromagnet (blue) or bi-layered antiferromagnet (red).

The strong (*a*,*b*) planar anisotropy induced by the crystal field and the predominance of the dipolar interaction on the exchange coupling between the moments make the Bi-Layered AntiFerroMagnetic (or BLAFM) more energetically favorable. For this BLAFM structure, several equivalent configurations may occur: either all the moments are aligned along the *a* axis, or all along the *b* axis, or a coherent superposition of the two. In fact, at zero external field, the crystal is divided into several domains and each domain adopts a configuration. But a very low external field of 300 Oe applied along the *a* (respectively *b*) axis is sufficient to fix the orientation of moments along the *b* (respectively *a*) axis. This "crossover" is not interpreted as a phase transition but rather a redistribution of domains. One can observe a true phase transition by applying a transverse field $H_c = 4.03kOe$ along the *c* axis.

Various experimental studies have been conducted by the LQM on this compound. They have allowed to establish, inter alia, the critical exponents of the phase transitions $\alpha = -0.28 \pm 0.04$, $\beta = 0.15 \pm 0.02$, $\delta = 15.2$ and $\eta = 0.26$ [16] which belong to the universality class of two-dimensional model. However, the Mermin-Wagner theorem excludes any ordering on a large scale in a purely 2D XY model (although a weak anisotropy h_4 leads to the appearance of a conventional order slightly above the Kosterlitz-Thouless transition). As for the quantum phase transition, the observed order parameter exponent $\beta = 0.31$ is consistent with a classical 3D scaling, which is coherent with the Hertz result stating that a quantum phase transition in a *d*-dimensional system (2D XY/h_4 here) scales as a classical system in *d+1* dimensions [11].

Finally the appearance of an ordered phase in $LiErF_4$ could be explained by the phenomenon of "order by disorder", by conducting a similar reasoning to that of Henley [10] to the $LiErF_4$ lattice which is actually a distorted version of a diamond-like lattice.

From a theoretical point of view, numerical simulations using the mean field approximation have failed to reproduce correctly the phase transition around the critical point, or to find these critical exponents specific to a 2D structure. Hence the need to try a new approach intended to simulate more accurately the mechanisms of frustration and phase transition, in this case a Monte Carlo simulation.

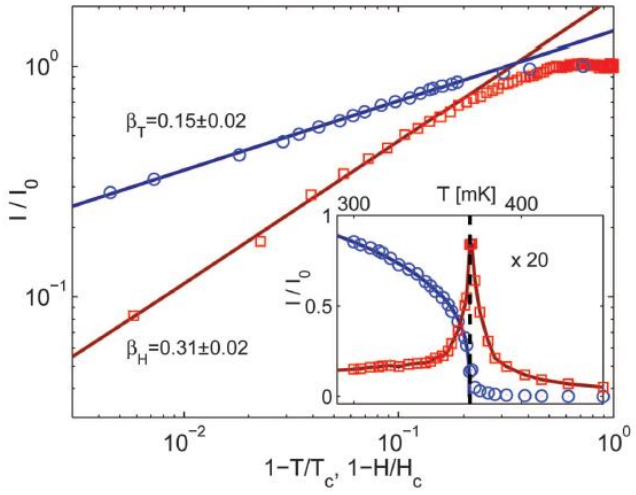

Figure 7 : Neutron scattering data of $LiErF_4$ [16]. (010) intensity as a function of temperature at H = 0 (blue circles) and a c axis field at T = 80mK (red squares). Lines are power law fits. (Inset) Intensity of Bragg peak (blue circles) and critical scattering (red squares) extracted by fitting a resolution-corrected sum of a delta function and a Lorentzian to crystal rotation scans.

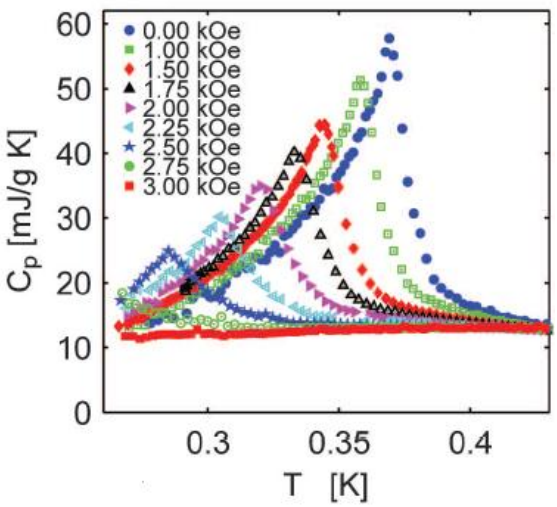

Figure 6 : Specific heat versus temperature for several fields along the *c* axis [16].

1.3. $LiHo_xEr_{1-x}F_4$

It is possible to grow crystals containing a mixture of rare earth rather than to use only a non-magnetic dopant. There is yet no scientific publication of such mixtures, although studies on the effects of off-diagonal coupling in $LiHo_xY_{1-x}F_4$ [23, 24, 27] suggest the development of these new materials.
Indeed, due to the XY planar anisotropy of $LiErF_4$, the moments of the erbium ions will be coupled to the moments of holmium ions via the off-diagonal terms of the dipole interaction matrix. It even seems that erbium is more effective than yttrium in this type of coupling, making possible the emergence of spin glasses at low dilutions.

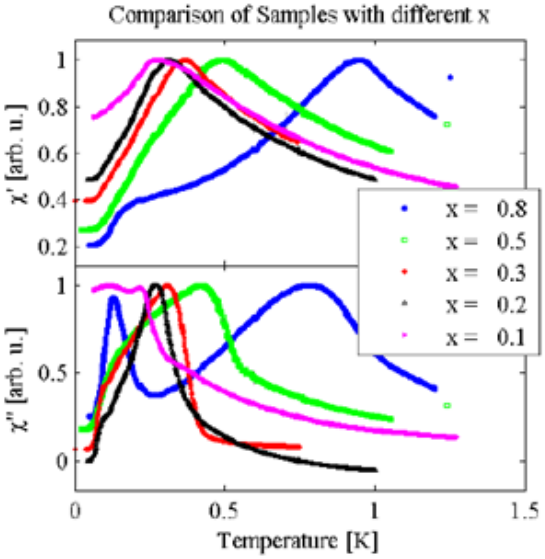

Figure 8 : Comparison of AC susceptibility scans of $LiHo_xEr_{1-x}F_4$ for different holmium proportions x [20].

Recent AC susceptibility measurements carried out at the LQM [20] allowed to reveal a conventional ferromagnetic order for $x>0.8$ and a spin-glass phase for $x<0.5$, while mean-field numerical simulations predict a long range magnetic order regardless of the dilution. Again, the mean field approach shows its limits. Neutron scattering experiments [17] have also shown that the transition to disordered phases is mainly due to short-range antiferromagnetic interactions.

2. THEORETICAL ASPECTS

A first step is to derive an effective model, that is to say, truncated to an Ising model of spins 1/2. This approach is possible because the first excited state is relatively far from the degenerate ground state doublet. This model should contain all the physics of the full system and be valid for all types of ions. The Monte Carlo simulations will be performed on this "reduced" system. The Hamiltonian describing the system can be written:

$$H = H_Z + H_{cf} + H_D + H_{hf} \tag{1}$$

with H_Z the Zeeman term, H_{cf} the crystal field Hamiltonian, H_D the dipolar interaction Hamiltonian and H_{hf} the hyperfine interaction.

- **Zeeman term**

  The simplest part of the single ion Hamitonian is the Zeeman term, describing the interaction between a magnetic moment $g_{Landé}\mu_B\mathbf{J}$ with a magnetic field **H**:

$$H_Z = -g_{Landé}\mu_B\mathbf{J}\cdot\mathbf{H} \tag{2}$$

  with **J** the spin operators vector $(\hat{\mathbf{J}}_x, \hat{\mathbf{J}}_y, \hat{\mathbf{J}}_z)$.

- **Crystal field**

  The charge distribution around an ion creates an electric field which acts on the *4f* electrons, resulting in a large anisotropy. The *crystal field* can then be written:

$$v_{cf} = \int \frac{e\rho(\mathbf{R})}{|\mathbf{r}\text{-}\mathbf{R}|}\mathrm{d}\mathbf{R} \tag{3}$$

  where $\rho(\mathbf{R})$ is the charge density. If this field does not penetrate the *4f* shell, then v_{cf} is given by solving the Laplace equations and can be expanded in spherical harmonics:

$$v_{cf} = \sum_{l,m} A_l^m\, r^l Y_{lm}(\hat{r}) \tag{4}$$

  By applying the Wigner-Eckart theorem, one can show [25, 26] that the matrix elements of v_{cf} are proportional to those of Racah operators $\tilde{R}_{lm}$ written in terms

of **J** operators. The crystal field can then be written by summing over all ions *i* of the considered system:

$$H_{cf} = \sum_i \sum_{l,m} A_l^m \alpha_l \langle r^l \rangle \left(\frac{2l+1}{4\pi}\right)^{0.5} \tilde{R}_{lm}(\mathbf{J}_i) \tag{5}$$

However, it is more common to use the Stevens operators (defined in Appendix 2), derived from tesseral harmonics:

$$H_{cf} = \sum_i \sum_{l,m} B_l^m \, \hat{O}_l^m(\mathbf{J}_i) \tag{6}$$

The B_l^m coefficients correspond to energies that can in principle be obtained from the charge distribution. However, in our case, this distribution is poorly understood and few attempts have met with little success [13]. Another possibility is to treat these coefficients as experimentally determined parameters. The S_4 point symmetry of rare earth ions fortunately limits the number of these parameters:

$$H_{cf} = \sum_{l=2,4,6} B_l^0 O_l^0 + \sum_{l=4,6} B_l^4(c) O_l^4(c) + B_l^6(s) O_l^6(s) \tag{7}$$

Numerical values of the B_l^m coefficients can be found in Appendix 2 for different compounds. In $LiHoF_4$, a negative B_2^0 leads to the strong *z* axis Ising anisotropy, whereas a positive B_2^0 leads to the planar XY anisotropy in $LiErF_4$.

- **Dipolar interaction**

In general, the interaction between two ions *i* and *j* can be written:

$$H_D = \sum_i \sum_j \mathbf{J}_i^+ L(i,j) \, \mathbf{J}_j \tag{8}$$

where $L(i,j)$ is a 3x3 tensor. For example, for the Heisenberg exchange term, which is isotropic, $L(i,j)_{\alpha\beta} = J_{ex}\delta_{\alpha\beta}$ with $\alpha, \beta = x, y, z$.
In this formalism, the tensor of the dipolar interaction, which is anisotropic, can be written:

$$L(i,j) = -\frac{\mu_0}{4\pi}(g_{Landé}\mu_B)^2 \frac{N}{V} D(i,j) \tag{9}$$

where $D(i,j)$ is a dimensionless tensor given by:

$$D_{\alpha\beta}(i,j) = \frac{V}{N}\frac{3\left(\mathbf{R}_{j\alpha} - \mathbf{R}_{i\alpha}\right)\left(\mathbf{R}_{j\beta} - \mathbf{R}_{i\beta}\right) - \delta_{\alpha\beta}\left|\mathbf{R}_j - \mathbf{R}_i\right|^2}{\left|\mathbf{R}_j - \mathbf{R}_i\right|^5} \tag{10}$$

The dipolar interaction has a very long range effect and is highly anisotropic, and dealing with it in a finite size system should therefore be done with care.
Its spatial Fourier transform is:

$$D_{\alpha\beta}(q) = \frac{1}{N}\sum_i \sum_j D_{\alpha\beta}(i,j) e^{-iq(\mathbf{R}_i - \mathbf{R}_j)} \tag{11}$$

Considering the limit $q = 0$ and setting $\boldsymbol{r} = \mathbf{R}_i - \mathbf{R}_j$, it is possible to separate the sum over *j* in a discrete sum over the lattice (limited to a sphere) and a continuous sum for large $\boldsymbol{r}$ (from the lattice boundaries to the surface of the crystal):

$$\sum_j \ldots = \sum_{j \in sphere} \ldots + \frac{N}{V}\int_{sphere}^{cristal} \ldots \, \mathrm{d}\boldsymbol{r} \tag{12}$$

The detailed calculation in the work of J. Jensen and A. R. Mackintosh [13] p. 222-223 shows that the integrals for α ≠ β vanish by symmetry and only the diagonal terms remain:

$$\int_{sphere}^{\infty} \ldots \, \mathrm{d}\boldsymbol{r} = \frac{4\pi}{3} - N_d \tag{13}$$

where $\frac{4\pi}{3}$ is the contribution of the surface of the sphere (Lorentz term) and N_d is the demagnetization term (contribution of the surface of the sample). These two terms are the source of long-range character of the dipolar interaction, especially in the case of $LiHoF_4$ where the Lorentz term dominates and is responsible for the ferromagnetic ordering.

- **Hyperfine interaction**

The hyperfine interaction between the *4f* moments and the nuclear spin **I** can be written:

$$H_{hf} = A\sum_i \mathbf{I}_i \cdot \mathbf{J}_i \tag{14}$$

But most of the time A is of the order of $10^{-6}eV$ and has very little influence, except for $LiHoF_4$ at low temperature and high fields.

2.1. Mean field approximation

Before tackling the development of the Monte Carlo code, we need a benchmark for developing the effective model. It is therefore necessary to perform simulations based on a theory easier to implement but which still takes into account the many-body system. The mean field theory replaces the interactions between various ions by interaction between a single ion with a self-consistent field, neglecting fluctuations of the moments around their equilibrium position. We can write the mean field Hamiltonian as follows:

$$H_n^{MF} = \mathbf{J}_n \cdot \mathbf{H}_n + H_{cf} + A\, \mathbf{I}_n \cdot \mathbf{J}_n \tag{15}$$

where n is the index of the sites (or ions) within the unit cell, H_{cf} is the crystal field Hamiltonian, A is the hyperfine coupling and $\mathbf{H}_n$ the mean field of the site n given by:

$$\mathbf{H}_n = \sum_{m(n)} \mathcal{J}_{12} \langle \mathbf{J}_m \rangle + \sum_m \frac{\mu_0}{4\pi} (g_{Landé}\mu_B)^2 \, D_{mn}(\mathbf{q}=0) \langle \mathbf{J}_m \rangle \tag{16}$$

with :

$$D_{mn}(\mathbf{q}=0) = \frac{N}{V}\left(\frac{4\pi}{3} + \left[\underline{D}_{mn}(\mathbf{q}=0)\right]_L - N_d\right) \tag{17}$$

where $\frac{4\pi}{3}$ is the Lorentz term, $[D_{mn}(\mathbf{q}=0)]_L$ the dipolar sum over a lattice L of finite volume and N_d the demagnetization factor. N is the number of ions per unit cell, and V the volume of a unit cell.
The fixed-point algorithm takes one unit cell and performs the following tasks:

1. The magnetic dipolar interaction $\underline{D}_{mn}(\mathbf{q}=0)$ is first summed for all ions located inside a sphere centered on the unit cell and which radius is fixed in order to obtain a sufficiently accurate result without sacrificing computing time. Then moments $\mathbf{J}_m$ of the unit cell are initialized in a certain configuration. These two operations are executed only once at the beginning of the calculation.
2. The mean fields $\mathbf{H}_n$ are computed according to the current moments' configuration.
3. The mean moments $\langle \mathbf{J}_m \rangle$ are updated by computing the thermal average from the eigenvalues and eigenvectors of H_n^{MF} :

$$\langle \mathbf{J}_m \rangle = \frac{1}{Z} \sum_i \sum_\lambda \langle \lambda | \mathbf{J}_{i,m} | \lambda \rangle \, e^{-\beta E_\lambda} \tag{18}$$

with Z the partition function and $\beta = \frac{1}{k_B T}$

4. The algorithm then iterates steps 2 and 3 until the difference between the mean moments of the *i*-th step and those of the *(i+1)*-th step goes below a threshold of 10^{-6}, otherwise it stops automatically after 10 000 steps. This ensures a good overall convergence, even near the critical point where we can predict the starting point of the next loop with the help of curve fitting to approximate a law in $(T - T_C)^{-\frac{1}{2}}$.

Deep in the ordered phase, the mean field calculation should work. But towards to the phase transition, as fluctuations gain in importance, this approximation may not truly render the phase transition.

2.2. Effective model

The crystal field H_{cf}, when diagonalized, gives rise to a degenerate ground state separated by 2.214meV (or 25.7K) from the first excited state in the case of $LiErF_4$, and more than 10K in the case of $LiHoF_4$. It is therefore possible to build an effective Hamiltonian from the single-ion terms H_{cf} and H_Z, restricted to the doublet $\{|1\rangle, |2\rangle\}$ and chosen such as it diagonalizes $\hat{\mathbf{J}}_z$:

$$\langle i | \hat{\mathbf{J}}_z | j \rangle = j_z \hat{\mathbf{S}}_z \tag{19}$$

with $\hat{\mathbf{S}}_z$ the usual spin operator. We can then build effective spin operators:

$$\tilde{\mathbf{J}}_\alpha = \langle i | \hat{\mathbf{J}}_\alpha | j \rangle \tag{20}$$

If the doublet is degenerated (i.e. in the case of a zero field), it is still necessary to rewrite the effective operators in a suitable base, such as the eigenvectors of $\tilde{\mathbf{J}}_Z$ for example. As $\tilde{\mathbf{J}}_\alpha$ is a 2x2 Hermitian matrix, it can then be written in the basis formed by the Pauli matrices σ_β and the identity matrix σ_0:

$$\tilde{\mathbf{J}}_\alpha = \sum_\beta g_{\alpha\beta} \sigma_\beta + a_\alpha \sigma_0 \tag{21}$$

with

$$g_{\alpha\beta} = \frac{1}{2} Tr\left(\sigma_\beta \tilde{\mathbf{J}}_\alpha\right) \tag{22}$$

and

$$a_\alpha = \frac{1}{2} Tr\left(\tilde{\mathbf{J}}_\alpha\right) \tag{23}$$

One therefore gets

$$\tilde{\mathbf{J}} = G\hat{\mathbf{S}} + \mathbf{a} \tag{24}$$

with

$$\hat{\mathbf{S}} = \begin{pmatrix} \sigma_x \\ \sigma_y \\ \sigma_z \end{pmatrix} \tag{25}$$

H_{cf} and H_Z allow the derivation of effective spin operators, but they still generate two terms:

$$e_B = \lambda_1 - \lambda_2 \tag{26}$$

$$C = \lambda_1 + \lambda_2 \tag{27}$$

where λ_1 et λ_2 are the first two eigenvalues of $H_{cf} + H_Z$.
Ideally, $\tilde{\mathbf{J}}_x = j_x \sigma_x$ and $\tilde{\mathbf{J}}_y = j_y \sigma_y$ where j_x and j_y are purely real. If this is not the case, the non-zero phases of the complex matrix elements of $\tilde{\mathbf{J}}_x$ and $\tilde{\mathbf{J}}_y$ will yield off-diagonal coefficients in the G tensor. By applying rotations on $\tilde{\mathbf{J}}_x$ and $\tilde{\mathbf{J}}_y$, it is possible to obtain a G tensor of the following form:

$$G = \begin{pmatrix} g_\parallel & 0 & 0 \\ 0 & g_\parallel & 0 \\ 0 & 0 & g_\perp \end{pmatrix} \tag{28}$$

In the case of $LiErF_4$, $g_\parallel = 6.5614$ and $g_\perp = 3.2319$.
The dipolar interaction then becomes:

$$\tilde{H}_D = \sum_{i \in ions} \sum_{j \in ions} \left(\hat{\boldsymbol{S}}_i^+ G^T + \boldsymbol{a}^T\right) D(i,j) \left(G\,\hat{\boldsymbol{S}}_j + \boldsymbol{a}\right) \tag{29}$$

In practice, we will work within the classical limit by replacing $\widehat{\boldsymbol{S}}_i$ with the *i*-th ion's moment $\boldsymbol{\mu}_i$:

$$\widetilde{H}_D = -\frac{1}{2}\sum_{i\,\in\,ions}\sum_{j\,\in\,ions} g^i_{Landé} g^j_{Landé} (\boldsymbol{\mu}_i^T G^T + \boldsymbol{a}^T) D(i,j) \left(G\,\boldsymbol{\mu}_j + \boldsymbol{a}\right) \tag{30}$$

The Zeeman term and the crystal field Hamiltonian become:

$$\widetilde{H}_Z + \widetilde{H}_{CF} = -\sum_i (e_B \mu^i_\alpha) + C \tag{31}$$

where μ^i_α is the α component of the *i*-th ion's moment, α corresponding to the direction in which the field is applied.
For a given ion *i* the dipolar interactions are summed over all ions *j* that lie within a sphere of a certain radius:

$$\widetilde{H}_D = -\frac{1}{2}\sum_{ij}\sum_{\mathbf{R}\,\in\,\text{sphère}} g^i_{Landé} g^j_{Landé} (\boldsymbol{\mu}_i^T G^T + \boldsymbol{a}^T) D(\boldsymbol{\tau}_{ij} + \mathbf{R}) \left(G\,\boldsymbol{\mu}_j + \boldsymbol{a}\right) \tag{32}$$

with $\boldsymbol{\tau}_{ij}$ the translation vector between ion *i* and ion *j* within the same unit cell, and **R** the translation vector between unit cells.
The effective Hamiltonian is finally written:

$$\widetilde{H}_{tot} = \widetilde{H}_D + \widetilde{H}_Z + \widetilde{H}_{CF} \tag{33}$$

It is possible to improve the execution speed and accuracy of calculation, at the cost of memory use, on the assumption that $\boldsymbol{\tau}_{ij}$ is the translation vector between the ion *i* and ion *j* within the system considered (a cube of NxNxN unit cells) and that **R** is the translation vector between the system and its surrounding virtual replicas. Thus, the sum

$$\sum_{\mathbf{R}\,\in\,\text{sphère}} D(\boldsymbol{\tau}_{ij} + \mathbf{R}) \tag{34}$$

can be calculated only once at the beginning of the algorithm for each pair of ions (*i*,*j*). Dipolar interactions matrices are then indexed as a function of $\boldsymbol{\tau}_{ij}$ in a unique way in order to be able to access them afterwards just by knowing $\boldsymbol{\tau}_{ij}$. Note that this time, the dipolar matrices (17) are computed the following way:

$$D_{mn}(\mathbf{q}=0) = \left(\left[\underline{D}_{mn}(\mathbf{q}=0)\right]_L + \frac{4\pi}{3V} - N_d\right) \tag{35}$$

with *V* the total volume of the system, and now *N=1* because we consider only one ion per replica. The demagnetization factor will be ignored.
The matrices are then stored in memory and used when the energy is computed. The sum is always performed within a sphere, otherwise the Lorentz factor wouldn't be the same.

2.3. Simulated annealing

A major drawback of Monte Carlo simulations is the fact that the algorithm can bring the system into a local minimum and never get out. The simulated annealing technique provides a simple mean to escape from this trap.
In its most basic version, it is an adaptation of the Metropolis-Hastings algorithm which consists in successively running Monte Carlo simulations for a series of decreasing values of temperature. So we let the system find its ground state for a given temperature T_i, then we run another Monte Carlo calculation for a temperature $T_{i+1} < T_i$ by using the ground state found for T_i as the new starting point.
The algorithm first randomly populates the lattice according to the doping ratios and initializes the moments of every ion. The moments orientations can be initialized randomly or specified by the user (if the magnetic order is already known) in order to speed up the convergence. The Monte Carlo algorithm then randomly selects one ion and applies a uniformly random rotation to its magnetic moment. In this way, we construct a Markov chain, and all the information necessary to determine the future state is contained in the current state. Thus, at each step the algorithm generates a new state, calculates the new internal energy of the system and decides whether to accept or reject it in the following way:

1. The algorithm computes the acceptance factor, which is the Boltzmann factor in our case :

$$a = e^{-\beta(\Delta E)} \tag{36}$$

2. If $T = 0K$, the new state is accepted only if $\Delta E < 0$.
3. If $T > 0K$,
    - If $a \geq 1$, the new state is accepted.
    - Otherwise, a random number r is chosen in $\mathcal{U}(0,1)$. If $r \leq a$, l the new state is accepted, otherwise it is rejected.

The higher the temperature, the higher the probability of accepting a state of higher energy. Thus, starting the simulated annealing at temperatures of the order of mK allows the system to make leaps of energy high enough to escape a local minimum, while the Boltzmann distribution ensures that this local minimum will not be "visited" again. The

simulations being carried out within the effective model, it is important to keep the values of temperature and magnetic field relatively low so as to not get inconsistent results. Indeed, increasing these parameters would populate the excited levels, which are omitted in the effective model.

One would think that choosing a uniformly random rotation axis with a uniformly random rotation angle would result in a uniformly random rotation tensor. However, such a scheme makes the rotated sample vectors cluster about their original orientation and the rotation is therefore not uniform.

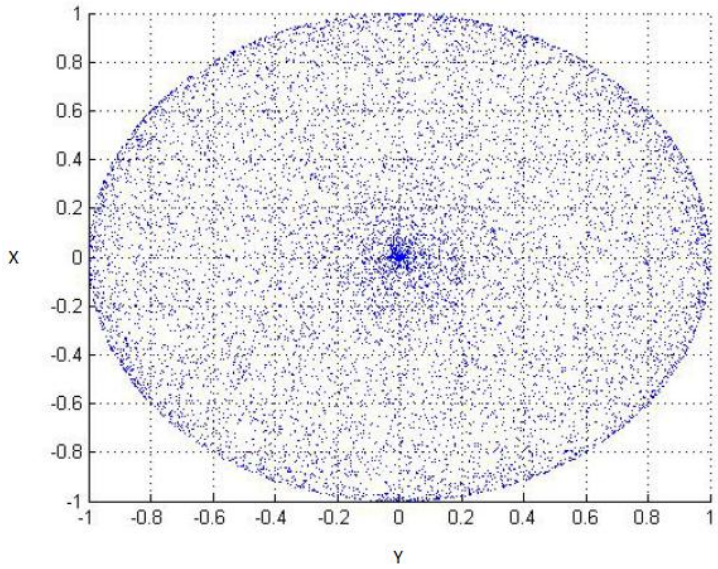

Figure 9 : Distribution of the vectors resulting from a "random" rotation of the $\hat{z}$ unit vector seen from above the unit sphere

Actually, uniform rotations require the distribution of the angle to be biased towards 180°, so that the expected value of the rotated vector is 0. The trick is to generate two uniformly random unit vectors, using Gram-Schmidt technique to orthonormalize them. A third unit vector is formed by a right-hand cross product of the orthonormal pair, and the rotation tensor is constructed by placing the three orthonormalized vectors into columns of the rotation tensor [3].

First we set $\mathbf{e_1}$ to be a uniformly random unit vector. We then construct a second uniformly random vector **m** and subtract away its part in the direction of $\mathbf{e_1}$:

$$\boldsymbol{e_2} = \frac{\boldsymbol{\mu}}{\|\boldsymbol{\mu}\|} \tag{37}$$

with

$$\boldsymbol{\mu} = \boldsymbol{m} - (\boldsymbol{m} \cdot \boldsymbol{e}_1)\boldsymbol{e}_1 \tag{38}$$

The third rotated unit vector is given by the right-hand cross product:

$$\boldsymbol{e_3} = \boldsymbol{e_1} \times \boldsymbol{e_2} \tag{39}$$

Finally, the rotation tensor is given by:

$$\boldsymbol{R} = (\boldsymbol{e_1}\, \boldsymbol{e_2}\, \boldsymbol{e_3}) \tag{40}$$

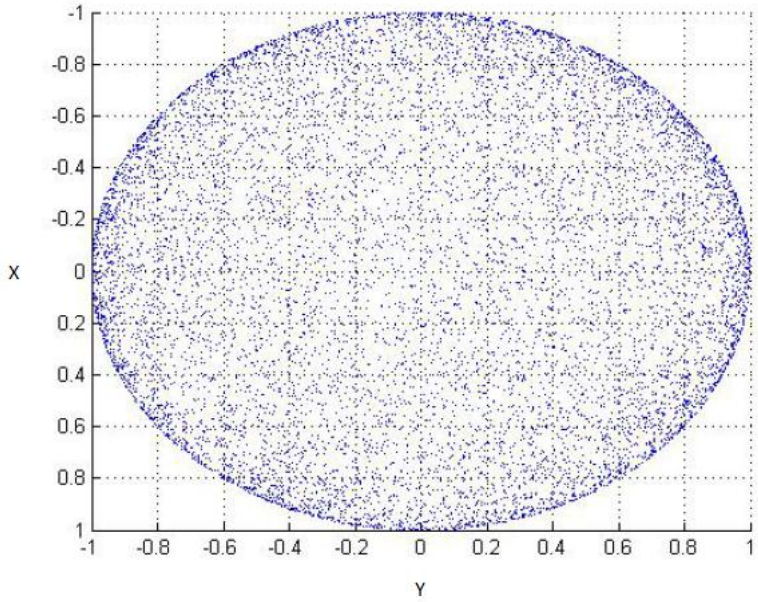

Figure 10 : Distribution of the vectors resulting from a true random rotation of the $\hat{z}$ unit vector seen from above the unit sphere

This method allows to perform true random rotations, but only to obtain uniformly distributed vectors. A smarter and faster way of performing the random rotation would be to use quaternions, which would also enable to control the final distribution of the rotated vectors.

For a given temperature it is expected that the system evolves in two stages. The algorithm will therefore be split into two parts:

- **Thermalization**

  The initial moments being randomly set up, the system is in a non-equilibrium state and will undergo a thermalization stage until it finds the ground state corresponding to the temperature. It is estimated that the system is thermalized when its internal energy no longer varies. The number of steps necessary for the system to reach equilibrium is function of its size and of the temperature decrement, and will therefore have to be determined. This part of the algorithm is

the fastest one, because it involves only the energy computation and the Metropolis criterion.

- **Measurements**

Once the system is thermalized, the algorithm starts measuring and storing the quantities of interest. On average, after N steps the Monte Carlo algorithm has modified N ions. These measures will be separated by as many steps as there are ions in the system and will be conducted over a large number of steps to obtain a significant statistical sample.

The order parameters measured here are the staggered magnetization along the *x* and *y* axes and the magnetization along the *z* axis, obtained by computing the scalar product of the four moments in each unit cell with:

$$X = \begin{pmatrix} 1 & 0 & 0 \\ -1 & 0 & 0 \\ -1 & 0 & 0 \\ 1 & 0 & 0 \end{pmatrix},\ Y = \begin{pmatrix} 0 & 1 & 0 \\ 0 & 1 & 0 \\ 0 & -1 & 0 \\ 0 & -1 & 0 \end{pmatrix},\ Z = \begin{pmatrix} 0 & 0 & 1 \\ 0 & 0 & 1 \\ 0 & 0 & 1 \\ 0 & 0 & 1 \end{pmatrix} \tag{41}$$

The order parameters squared are also computed and stored for further calculations.

The energy is given directly by (33), but the nested sum is only necessary at the first step. At each step only one moment is modified, therefore only the interactions involving this particular moment need to be computed again, that is the dipolar interactions with the other moments and the Zeeman term if an external field is applied. This trick accelerates considerably the calculation because the nested sum becomes a single sum:

$$-\frac{1}{2}\sum_{i\,\in\,ions}\sum_{j\,\in\,ions} g^i_{Landé} g^j_{Landé} (\boldsymbol{\mu}_i^T G^T + \boldsymbol{a}^T) D(i,j) \left(G\,\boldsymbol{\mu}_j + \boldsymbol{a}\right) \tag{42}$$

$$\rightarrow -\sum_{i\,\in ions} g^i_{Landé} g^j_{Landé} (\boldsymbol{\mu}_i^T G^T + \boldsymbol{a}^T) D(i,j) \left(G\,\boldsymbol{\mu}_j + \boldsymbol{a}\right)\Big|_j$$

The difference between the previous interactions and the new ones gives the energy difference used in the Metropolis criterion:

$$\Delta E = \left(\widetilde{H}_D + \widetilde{H}_Z\right)^{new} - \left(\widetilde{H}_D + \widetilde{H}_Z\right)^{old} \tag{43}$$

The square of the energy is also recorded.

It is also possible to confront the results with some neutron scattering data by computing the static structure factor, which is the discrete Fourier transform of the moments autocorrelation function, given by:

$$S^{\alpha\beta}(\boldsymbol{Q}) = \frac{1}{N}\sum_{jj'} e^{i\boldsymbol{Q}(\boldsymbol{R}_j - \boldsymbol{R}_{j'})}\langle \mu_j^{\alpha}\mu_{j'}^{\beta}\rangle \tag{44}$$

where $\boldsymbol{Q} = \boldsymbol{k}_{incident} - \boldsymbol{k}_{scattered}$ denotes the scattering vector, $\boldsymbol{k}$ being the neutron wave vector. The summation runs over all pair of spins in the lattice.
For $\boldsymbol{Q} = (0,0,0)$, $S^{\alpha\beta}(\boldsymbol{Q})$ is just the order parameter squared. But we will also compute $S^{\alpha\beta}(\boldsymbol{Q})$ for a small ΔQ along the *x* and *y* axes, with $\Delta Q = \frac{2\pi}{L}$. L being the size of the system, the fluctuations should be measured accurately for large systems only.
One can rewrite $S^{\alpha\beta}(\boldsymbol{Q})$:

$$S^{\alpha\beta}(\boldsymbol{Q}) = \frac{1}{N}\sum_{jj'} e^{i\boldsymbol{Q}(\boldsymbol{R}_j - \boldsymbol{R}_{j'})}\langle \mu_j^{\alpha}\rangle\langle \mu_{j'}^{\beta}\rangle + \frac{1}{N}\sum_{jj'} e^{i\boldsymbol{Q}(\boldsymbol{R}_j - \boldsymbol{R}_{j'})}\left\langle \left(\mu_j^{\alpha} - \langle \mu_j^{\alpha}\rangle\right)\left(\mu_{j'}^{\beta} - \langle \mu_{j'}^{\beta}\rangle\right)\right\rangle \tag{45}$$

The first term describes Bragg scattering, while the second one denotes the diffuse scattering, originating for example from finite size clusters or critical scattering close to the phase transition.
For each temperature, the energy, the energy squared, the moments, the moments squared, and the instantaneous structure factors are averaged over the sampling.

The fluctuation-dissipation theorem allows computing the specific heat and the magnetic susceptibility from thermal averages without differentiating any quantity.
One can use the following formulas:

$$C_{FDT} = \frac{1}{k_B T^2}\left(\langle E^2\rangle - \langle E\rangle^2\right) \tag{46}$$

$$\chi_{FDT}^{\alpha\beta} = \frac{1}{T}\left(\langle M^{\alpha}M^{\beta}\rangle - \langle M^{\alpha}\rangle\langle M^{\beta}\rangle\right) \tag{47}$$

where M^{α} is the α component of the magnetization.
The specific heat and the magnetic susceptibility can also be computed in the following way:

$$C_v = \frac{E(T+\Delta T) - E(T)}{\Delta T} \tag{48}$$

$$\chi^{\alpha\beta} = \frac{1}{T}\left(S^{\alpha\beta}\left(\boldsymbol{Q} = (\boldsymbol{0},\boldsymbol{0},\boldsymbol{0})\right)\right) = \frac{1}{NT}\sum_{jj'}\langle \mu_j^{\alpha}\mu_{j'}^{\beta}\rangle\Big|_T \tag{49}$$

with N the number of ions. The magnetic susceptibility and the specific heat are of great interest since they are experimentally more accessible than the magnetization or than the internal energy which cannot be directly measured.
Finally, for each temperature, the angles formed by each moment with the *a* axis are measured. This will be useful to plot angular distribution in the (*a*,*b*) plane or to follow the orientation of a particular moment (or four moments in a particular unit cell) during the phase transition.

The parts of the algorithm for the distribution of the ions, initialization parameters, the Metropolis-Hastings criterion and the measurements on the system will be implemented with MATLAB.
Those requiring more computational power like the rotation of the moments, the calculation of the dipole interaction matrix, and the calculation of energy will be coded in C. The functions implemented in C will have to be interfaced with the MATLAB software using the MEX functions and some of them will be parallelized. The computation of the order parameters and of the moments autocorrelation function Fourier transform is done under MATLAB using a vectorized code, which is actually even faster than doing **for** loops in C if the data is stored as a vector (that is, in contiguous locations in the computer's memory).

3. RESULTS

We discuss here the validity of the effective model and we present the results obtained with the mean field algorithm and the simulated annealing procedure presented in chapter 2.

3.1. Mean field approach

In the case of $LiErF_4$, the moments are initialized in the BLAFM configuration at zero temperature and zero external magnetic field. The wise order parameter to observe is the staggered magnetization, which alternates sign for each site according to the BLAFM structure, in order to measure the antiferromagnetic ordering. By increasing the temperature in zero field we obtain:

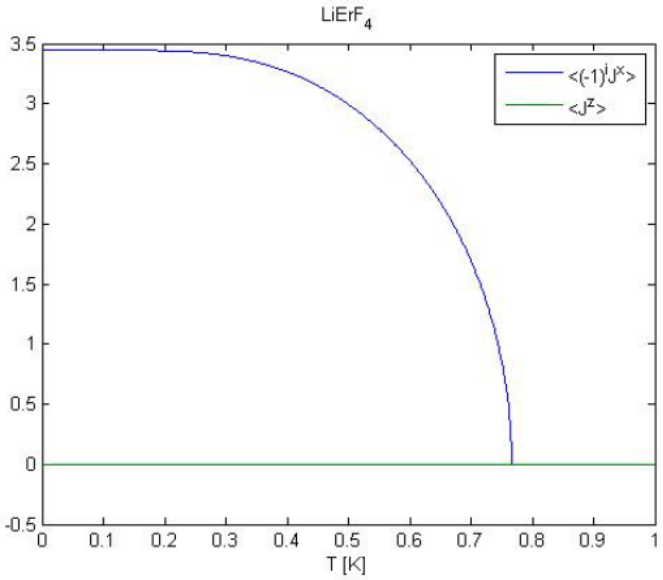

Figure 11 : Thermal phase transition of $LiErF_4$ (x component of the staggered magnetization in blue, and the z component of the magnetization in green) in the global model.

According to Fig. 11 $LiErF_4$ is an antiferromagnet below 767mK at zero field. But the mean field theory overestimates the critical temperature and many experiments show that it is only 373mK [20].

Another interesting result concerns the quantum phase transition, that is the one which occurs when varying the external magnetic field at zero temperature.
We want to observe the evolution of the staggered magnetization in the TFIM, we will therefore apply an external magnetic field perpendicular to the plane in which the moments are aligned (the (*a*,*b*) plane), that is along the *c* axis.

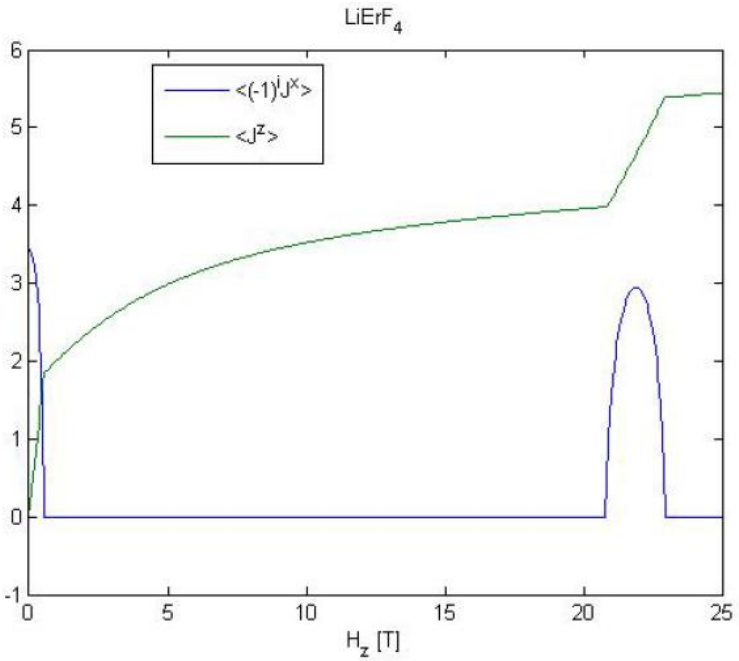

Figure 12 : Quantum phase transition of $LiErF_4$ (x component of the staggered magnetization in blue, and the z component of the magnetization in green).

There is a first quantum phase transition for $H_Z = 0.4T$, then a second at $H_Z = 20.8T$ and a third one at $H_Z = 23T$. This new antiferromagnetic phase, very surprising, is explained by the behavior of the crystal field energy levels.

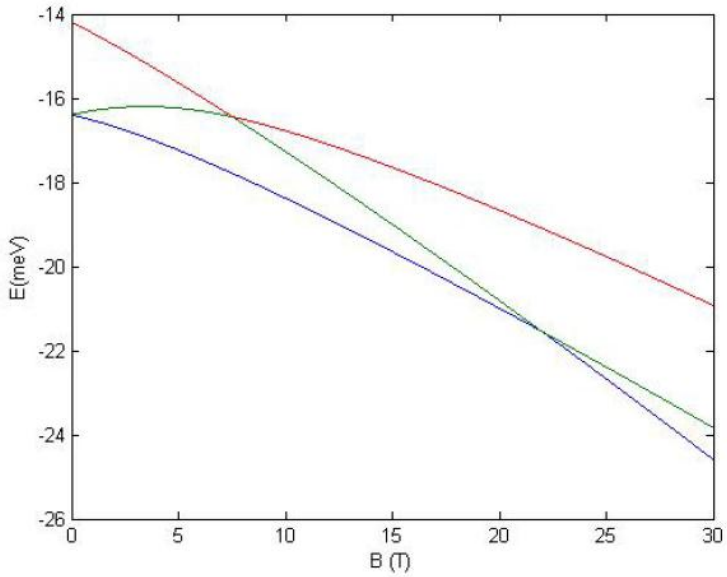

Figure 13 : Three first crystal field levels of $LiErF_4$as a function of the external magnetic field.

We note that the third energy level becomes the ground state at 22T. This yields an increase of the moments' length, which will in turn enhance the dipolar interactions between them and reactivate the antiferromagnetic order.

This result was considered very interesting and will be verified experimentally next year in another laboratory (the LNCMI in Grenoble) where we will measure, among other things, the magnetic susceptibility:

$$\chi_{\alpha\beta}(H,T) = \frac{M_\alpha(H + dh_\beta) - M_\alpha(H)}{dh_\beta} \tag{50}$$

with $\alpha, \beta = x, y, z$.
Assuming $dh_x = dh_y = dh_z$ and that the magnetic field is applied along z:

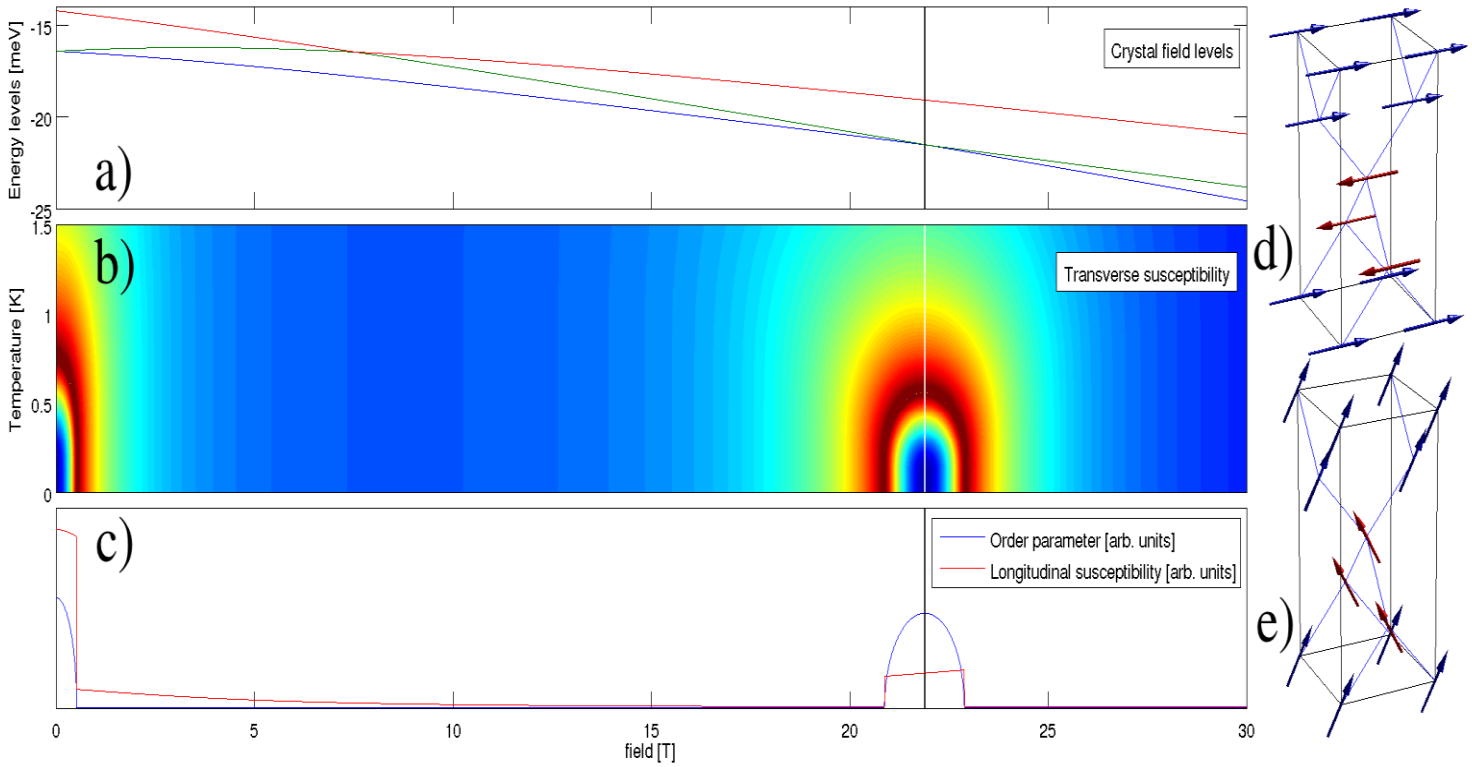

Figure 14 : a) Crystal field levels, b) Magnetic susceptibility as a function of the temperature and of the field, c) Staggered magnetization (blue) and DC susceptibility (red) as a function of the field, d) and e) Magnetic structures for a weak external field and for a strong one (respectively).

Although very promising and requiring to be verified experimentally, this phenomenon has not been deepened through my master thesis because the main goal of these mean field calculations is to build an effective model, which only works for weak magnetic field.
Phase transitions of other compounds ($LiYbF_4$, $LiGdF_4$ and $LiTmF_4$) were also calculated and are shown in Appendix 3, but are of no interest to the simulated annealing study of $LiHo_xEr_yY_{1-x-y}F_4$.

3.2. Effective model

- **$LiErF_4$**

Verification of the effective model was done in two stages. First, we consider a very simple system, namely a dimer located in a half-truncated unit cell (truncated along the c axis). It is thereby possible to exactly diagonalize the Hamiltonian of the dimer in the full Hilbert space and compare the evolution of energy levels as a function of external magnetic field with that of the energy levels of the effective Hamiltonian (reduced Hilbert space). The two Hamiltonians contain the crystal fields acting on each ion, the Zeeman term and the dipolar interaction between the ions and their replicas. A second check will consist in running a mean field calculation based on the effective model and comparing the results with those based on the global model. $LiErF_4$ being dominated by short-range interactions, dipolar interactions are only summed over 10 replicas in all directions. Summing over more replicas only increases the computing time without providing further accuracy.
The first verification is convincing:

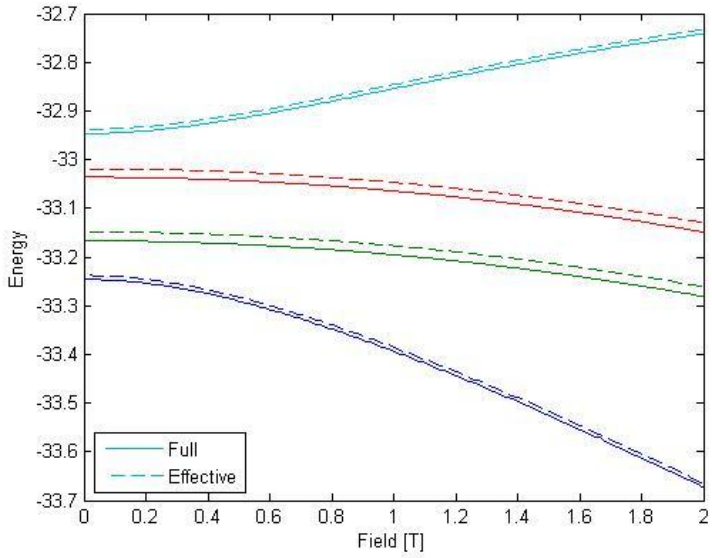

Figure 15 : Comparison of the energy levels (in meV) of an erbium dimer in the global model (solid line) and in the effective model (dashed line).

Energy levels appear similar in both models, only a slight shift of about $10\mu eV$ separates them. One can also compare the splitting of the ground state doublet in both models:

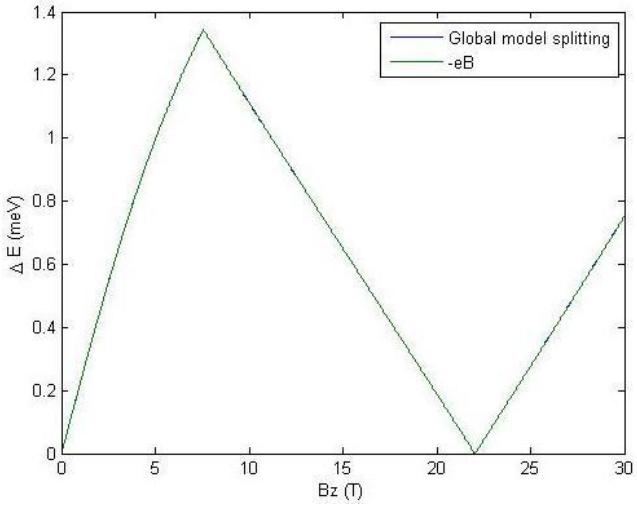

Figure 16 : Splitting of the ground state doublet of $LiErF_4$ in the global model (blue) and in the effective model (green).

Here the two curves overlap perfectly. The energy difference between the two lowest levels grows linearly up to 2-3T, then the crossing of the second and third energy levels leads to an anomaly at 7.5T. Finally the difference vanishes at 22.5T when the third level crosses the ground state.

The verification using mean field theory also gives results similar to the global model:

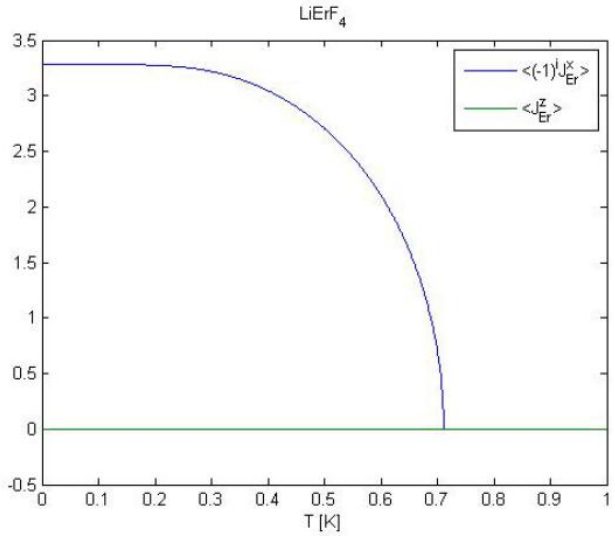

Figure 17 : Thermal phase transition of $LiErF_4$ (x component of the staggered magnetization in blue, and the z component of the magnetization in green) in the effective model.

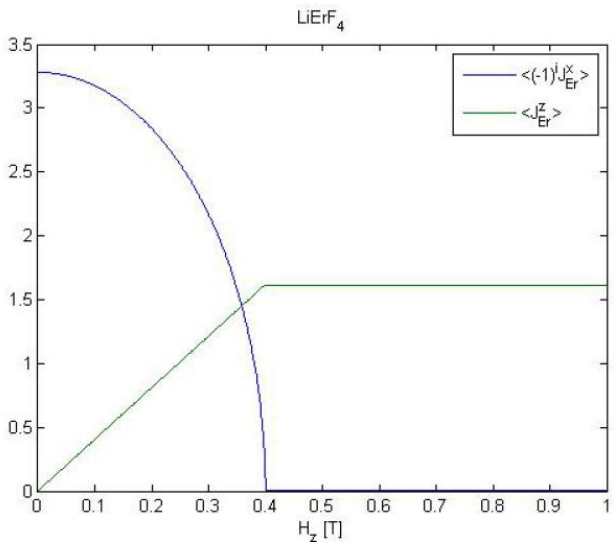

Figure 18 : Quantum phase transition of $LiErF_4$ in the effective model (transverse field).

It is found that the critical temperature and critical field have similar values in the global model (767mK and 400mT) and in the effective model (700mK and 390mT). This effective model is therefore validated for the $LiErF_4$ compound.

- **$LiHoF_4$**

Applying the same effective model on $LiHoF_4$ gives dubious results.

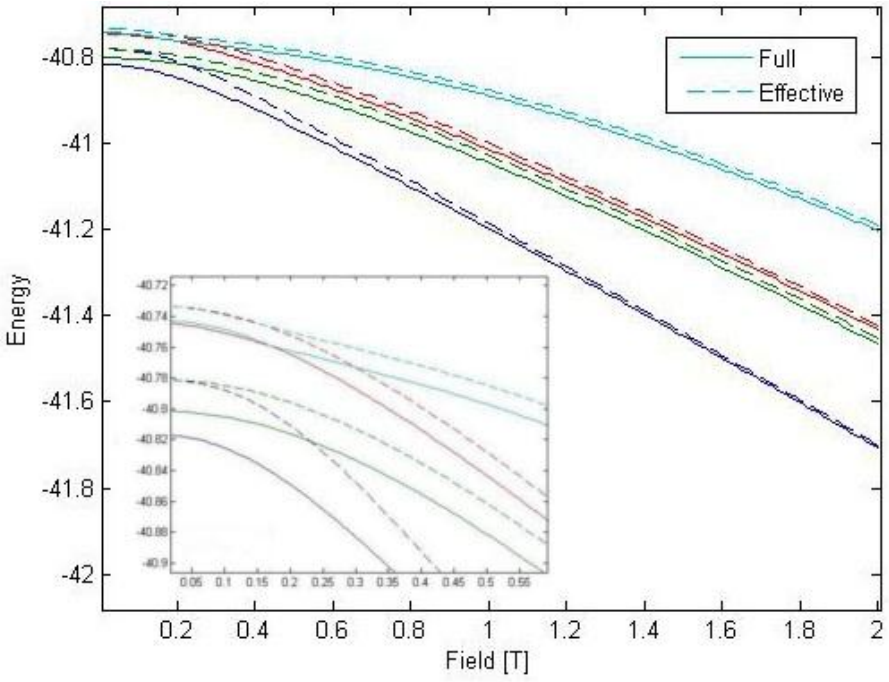

Figure 19 : Comparison of the energy levels (in meV) of a holmium dimer in the global model (solid line) and in the effective model (dashed line). (Inset) Zoom in the low fields region.

Although the energy levels behave similarly above 0.5T, they are completely different at low fields. The effective model even produces degenerated levels when the full model doesn't. We know that the magnetic ordering in $LiHoF_4$ is due to long range dipolar interactions, but summing them over more than 20 replicas doesn't change these results.
Many characteristics of the $LiHoF_4$ compounds can explain this. First of all, the derivation of the effective model parameters does not include the hyperfine coupling which at low temperature eventually mixes the 4f electron magnetic moments with the nuclear magnetic moment. It could explain the discrepancy, although it has been shown [2,22] that this coupling is determinant mainly at low temperature and high fields.

Also, the crystal field anisotropy of $LiHoF_4$ is less trivial than that of $LiErF_4$.

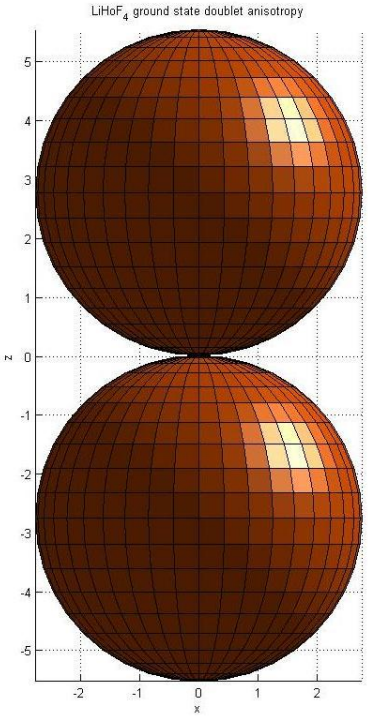

Figure 20 : Impact of the crystal field anisotropy on the ground state doublet of $LiHoF_4$.

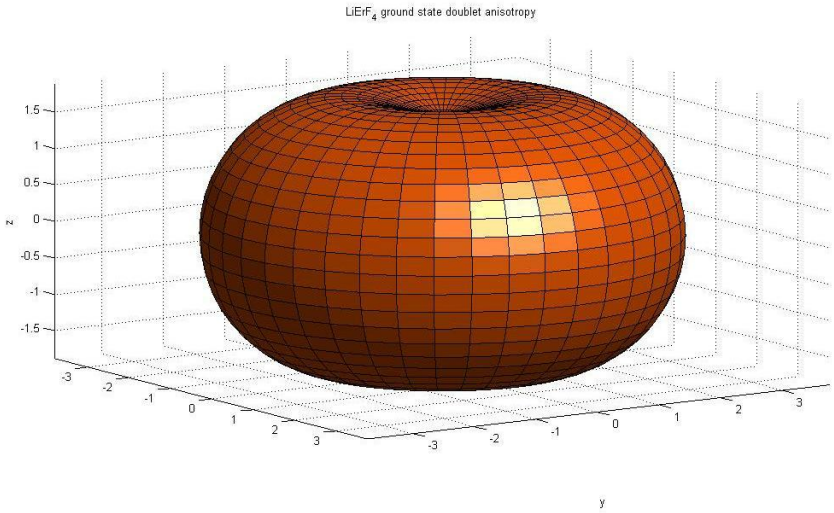

Figure 21 : Impact of the crystal field anisotropy on the ground state doublet of $LiErF_4$.

The anisotropy created by the crystal field on the ground state doublet of $LiHoF_4$ shows a pinch in the (*a*,*b*) plane. It may be that using a basic tensor formalism is not sufficient to describe this type of anisotropy.

3.3. Classical Monte Carlo calculations for $LiErF_4$

Intensive works dealing with Monte Carlo simulations have been conducted on $LiHo_xY_{1-x}F_4$ [7, 23, 27, 15, 1, 28] in order to determine whether the emergence of a spin glass can be predicted by the theory. But even for pure $LiHoF_4$, yet very well-known and widely discussed, there are still discrepancies between the theoretical and experimental results. P.B. Chakraborty *et al* [7] conclude that these discrepancies can be explained by mistakes in the mapping of the Ising model and its conformity with the actual material. A more recent study of S. M. B. Tabei *et al.* [27], using a Monte Carlo simulation of quantum perturbation, has reached to the same results, concluding that the discrepancies between theory and experiments do not come from programming errors.

As for the $LiHo_xY_{1-x}F_4$ dilutions, A. Biltmo *et al.* [1] determined the holmium proportions for which the ferromagnetic order disappears, but failed to highlight any spin glass freezing. The same study affirms that the crystal symmetry breaking is responsible for lowering T_c. It should be noted that the random fields generated by the dilution were omitted. Another study [28] claims to have found a spin glass transition at finite temperature using a Monte Carlo calculation, simultaneously run on multiple replicas, each one at different temperatures (a technique called "Parallel Tempering" or "Replica Exchange Markov Chain Monte Carlo ") with a Hamiltonian that takes only into account the dipolar interaction. This study estimates it takes 10^6 steps for the system to reach equilibrium.
However, there is to our knowledge no Monte Carlo simulation study that has been done on the $LiEr_xY_{1-x}F_4$ and $LiHo_xEr_{1-x}F_4$ compounds.

Given the long calculation time, it was decided that priority should be given to the establishment of the classical phase diagram of $LiErF_4$ to check if the theoretical critical exponents match the experimental ones found by C. Kraemer et al. [16].

For a system consisting of L^3 unit cells with L=4, one obtains:

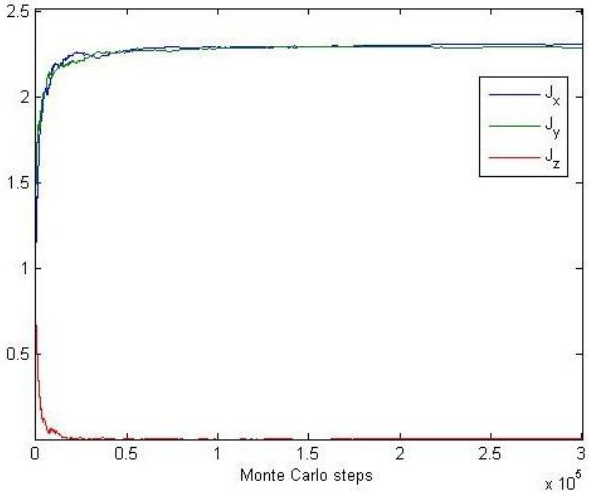

Figure 23 : Emergence of antiferromagnetic order in $LiErF_4$ at T=0K. J_x and J_y are the x and y component of the staggered magnetization per ion (blue and green, respectively), J_z is the z component of the magnetization.

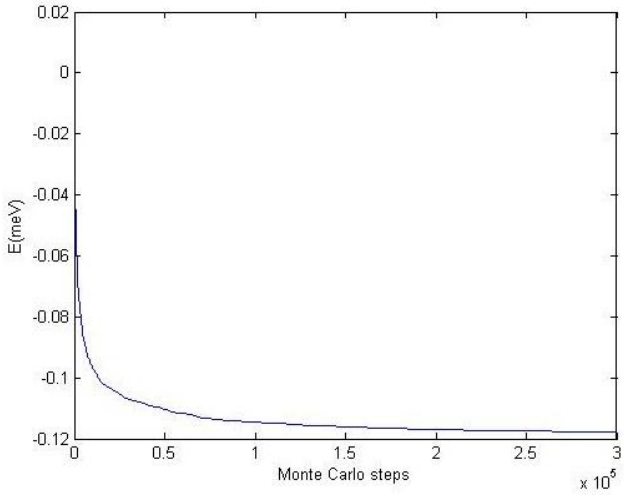

Figure 22 : Energy relaxation of $LiErF_4$ at T=0K. The ground state energy per ion at this temperature is -0.1226meV.

As expected, with zero external field the moments order antiferromagnetically in the (*a*,*b*) plane. As the energy decreases, the system goes from a random disordered phase (starting point) to the BLAFM structure. The *z* component of the magnetization is killed whereas the *x* and *y* components of the staggered magnetization slowly rise up to saturation ($\sqrt{J_x^2 + J_y^2} = 3.24\ while\ G_{xx} = G_{yy} = 3.2807$). As observed experimentally, the zero field structure is a distribution of domains where the moments lie in the (*a*,*b*) plane. Now, applying a small external field along *a* (or *b*) should fix all the moments along *b* (or *a*, respectively).

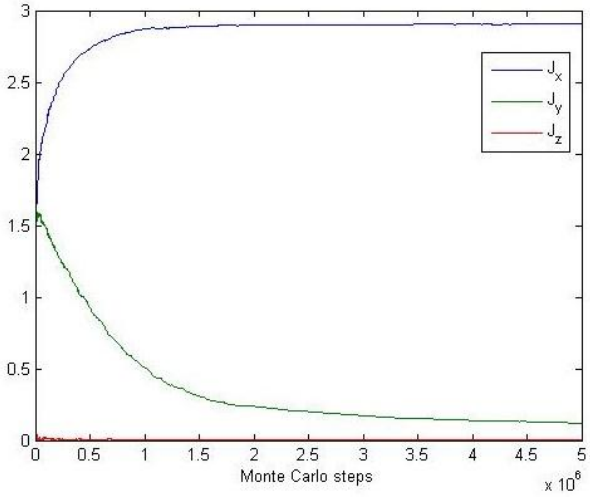

Figure 24 : Emergence of antiferromagnetic order in $LiErF_4$ at T=0K and H_y=0.06T. J_x and J_y are the x and y component of the staggered magnetization per ion (blue and green, respectively), J_z is the z component of the magnetization.

A very small field of at least 600Oe (instead of 300Oe experimentally) along *b* effectively suppresses the *b* axis domains. Moments parallel to the field are energetically less preferable than those lying perpendicular, because the latter can tilt towards the field with little cost of interaction energy. The moments are a little bit canted towards the *b* axis because of the field, but still tend to order antiferromagnetically along the *a* axis because the dipolar interaction is stronger than the Zeeman term.

Starting the Monte Carlo calculation from a high temperature and then slowly decreasing it ensures that the algorithm will bring the system to its real ground state at 0K, which is useful to study spin glasses and systems which ground state is unknown. However, it seems that increasing the temperature gives smoother and more realistic curves around the phase transition because it is easier for the algorithm to destroy order than to create it. Furthermore, the ground state of $LiErF_4$ at 0K is already known (BLAFM structure) and the goal of this study is to investigate what happens during the phase transition in a more accurate way than the mean field approximation. We will therefore start the simulation from the BLAFM ordering at 0K and slowly increase the temperature, using the simulated annealing code but for a set of increasing values of temperature. We know that the phase transition occurs at 373mK, we choose therefore forty temperature values between 0K and 1K. We will study the system for two different sizes: L=7 (that is 1372 ions) and L=10 (4000 ions). Numerical analysis of phase transitions and critical phenomena must be done carefully because sharp phase transitions occur only in the thermodynamic or infinite volume limit. Real macroscopic systems contain very large numbers of particles on the order of 10^{23}. They are much closer to the infinite volume limit than our computational systems, which typically involve 10^3 ions. The first thing to determine is the number of steps required to reach equilibrium, which depends on the size of the system and on the difference of temperature between two consecutive steps (0.04K in our case).

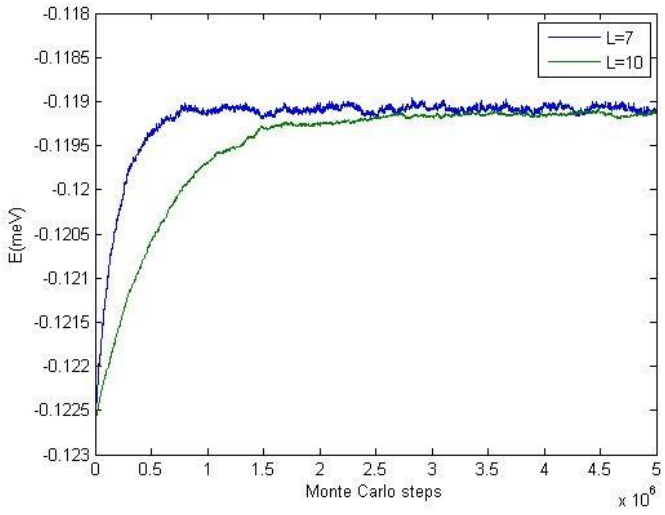

Figure 25 : Energy relaxation for dT=0.04K for L=7 (blue) and L=10 (green).

In Fig. 25, the system is initialized in the BLAFM structure at T=0K, and then the temperature is increased by 0.04K. Equilibrium is reached after $1,5.10^6$ steps for L=7 and

4.10^6 steps for L=10, meaning that every ion is visited a thousand times on average. Then, for each temperature value, statistics are collected every $4L^3$ step during another 2.10^6 steps run.

The following results have been calculated on a computer cluster enabling us to run many simultaneous calculations. For L=7, fifty independent equilibration runs were followed by two independent measurements runs for each equilibrated system, gathering one hundred independent realizations in ten days. For L=10, only five equilibration runs were completed before a maintenance on the server. They were followed by four measurements runs for each equilibrated system, gathering twenty independent realizations in nineteen days. Also the number of simultaneous calculations for L=10 was restricted because of memory limitations. We therefore emphasize that the data collected for L=10 may not be sufficient to compute results accurate enough, but they can still depict general behavior. The interesting order parameter here is the rotation invariant staggered magnetization in the (*a*,*b*) plane

$$J_{xy} = \sqrt{J_x^2 + J_y^2} \tag{51}$$

When computing its mean value $\langle J_{xy} \rangle$ and its standard deviation for each temperature over one hundred Monte Carlo calculations, one obtains the following phase transition

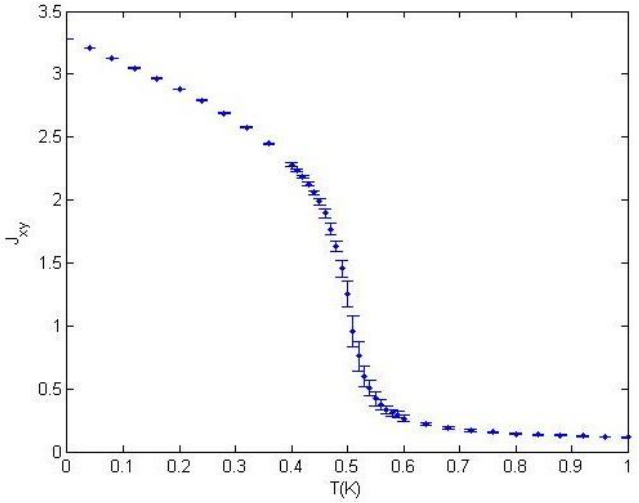

Figure 27 : Thermal phase transition of $LiErF_4$ obtained with the Monte Carlo method with L=7. The dots represent the mean values of J_{xy} over 100 calculations, error bars represent their standard deviation.

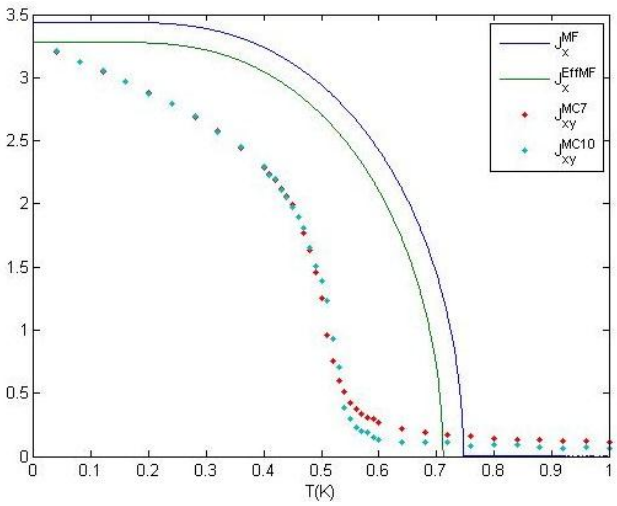

Figure 26 : Comparison of the mean field results (solid lines, in blue the global model, in green the effective model) with the Monte Carlo results (red dots were obtained with a system of L=7, cyan dots with L=10).

A first observation, very satisfying, is that the critical temperature is about 500mK which is closer to the experimental value (373mK) than the one given by the mean field approach (767mK). However, even after the occurrence of the phase transition at T_N, the magnetization still remains positive. This suggests that there is still some residual

alignment between the moments because of correlations. This occurs because the randomizing effect of temperature is not strong enough to create a completely random alignment between neighbouring moments. It could also be due to finite size effects, because this phenomenon is less important for L=10 than for L=7. The initial slope indicates that fluctuations already happen at really low temperatures.

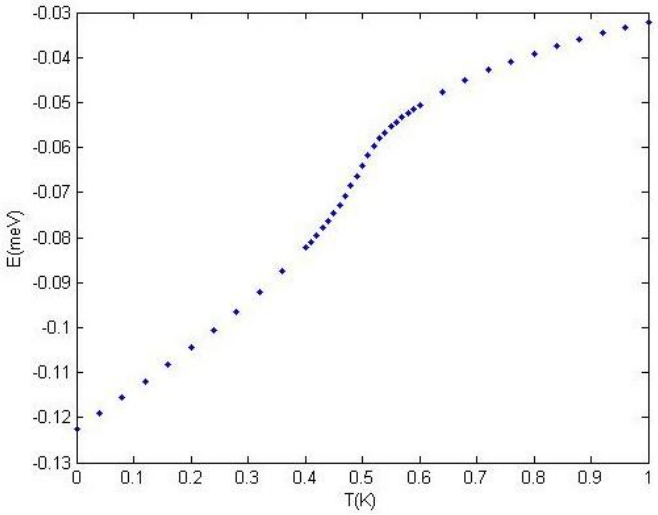

Figure 29 : Energy per ion during the thermal phase transition of $LiErF_4$ obtained with the Monte Carlo simulation with L=7.

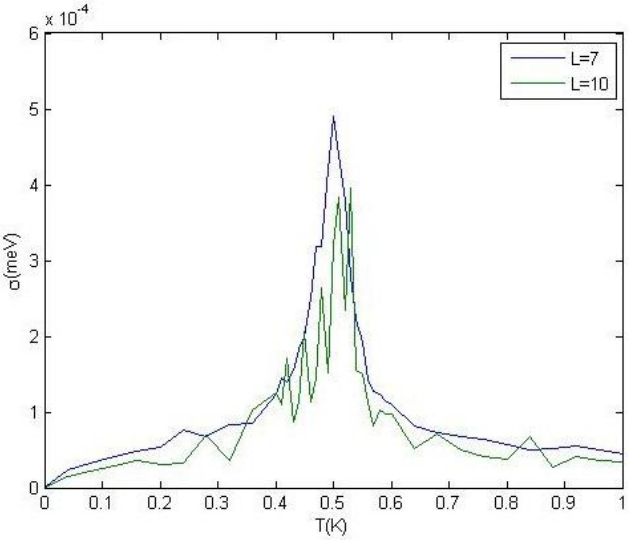

Figure 28 : Standard deviation of the energy as a function of the temperature for L=7 (blue) and L=10 (green).

Looking at Fig. 26, Fig. 27 and Fig. 29 it is really difficult to state what T_N exactly is. The fluctuations increasing around the phase transition, the standard deviation also increases around the critical point. This already gives an estimate for the critical temperature to be around 500mK. But quantities that become divergent at T_N like the magnetic susceptibility, the specific heat or the moments autocorrelation are much better for that.

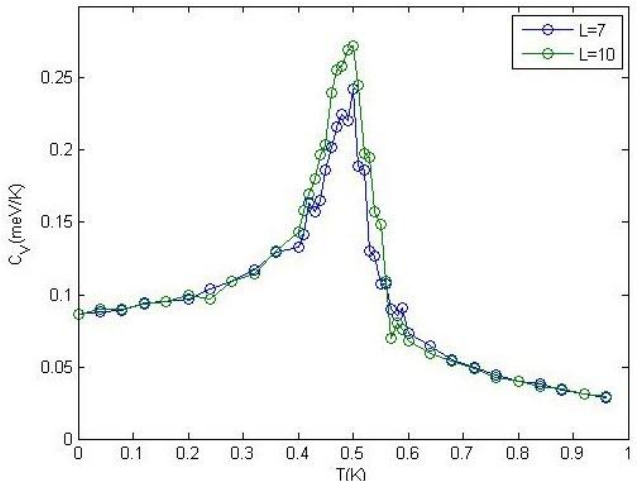

Figure 30 : Specific heat as a function of the temperature for L=7 (blue) and L=10 (green).

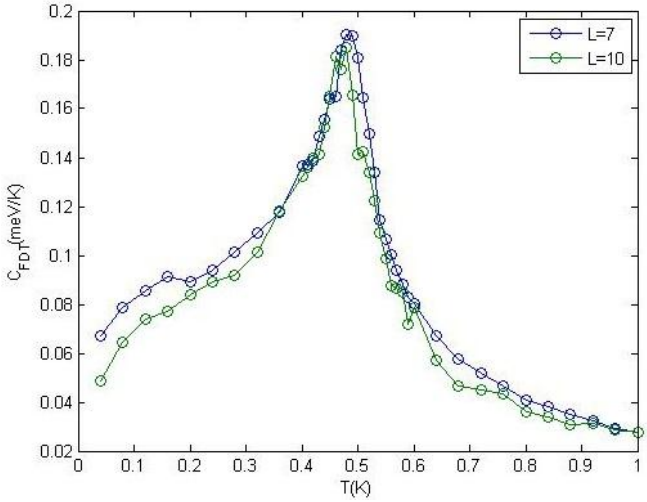

Figure 31 : Specific heat, computed from the fluctuation-dissipation theorem formula, as a function of the temperature for L=7 (blue) and L=10 (green).

As for the specific heat, there is not much difference between L=7 and L=10. For an infinite system, the specific heat diverges at T_N, but for finite size we only observe a peak due to the inflexion point in the energy. The specific heat derived from fluctuation-dissipation theorem (Fig. 31) shows a peak at *T=0.48K* for both sizes, while the specific heat computed by differentiating the energy (Fig. 30) exhibits a peak at *T=0.5K* for both sizes. Note that the shape of both specific heat is really close the experimental one (Fig. 7).

One can also compute the magnetic susceptibility in two different ways: from the moments autocorrelation's Fourier transform or from the fluctuation-dissipation theorem. Note that this enables us to investigate how the system would react to an external field without it becoming necessary to actually apply one.

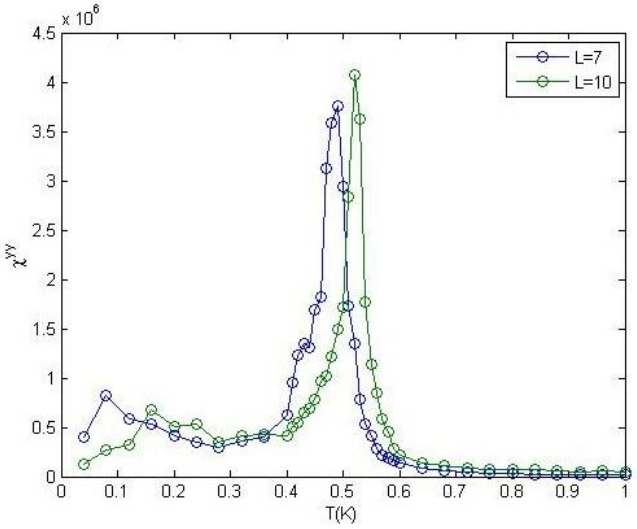

Figure 32 : Magnetic susceptibility as a function of the temperature for L=7 (blue) and L=10 (green).

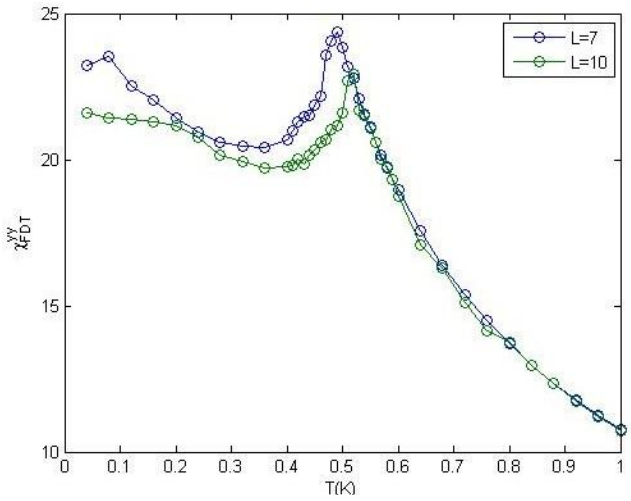

Figure 33 : Magnetic susceptibility, computed from the fluctuation-dissipation theorem formula, as a function of the temperature for L=7 (blue) and L=10 (green).

The magnetic susceptibility is another observable that is predicted to be divergent at the critical temperature, which reflects the correlation length divergence. The fact that it does not diverge but rather exhibits a peak (which still obeys a power law) may be due to the limited size of the system. For L=10 both approaches yield a susceptibility peak at *T=0.52K*, while for L=7 the peaks occur at *T=0.49K*.

The instantaneous structure factor provides an independent probe for the critical temperature. For $\boldsymbol{Q} = (0,0,0)$, one should expect $S^{\alpha\beta}(\boldsymbol{Q})$ to be the magnetization squared, which is what is actually measured with neutron scattering. In Fig. 34 is plotted $S(\boldsymbol{Q} = 0) = \sqrt{S^{xx}(0)^2 + S^{yy}(0)^2}$ which effectively corresponds to the staggered magnetization squared.

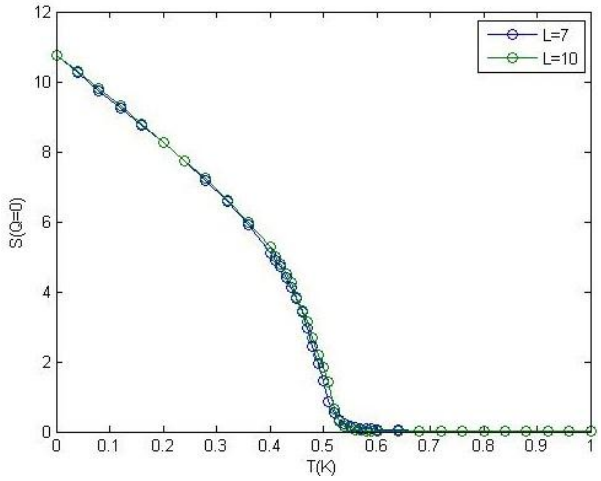

Figure 34 : In-plane moments autocorrelation Fourier transform for Q=(0,0,0), per spin, as a function of the temperature for L=7 (blue) and L=10 (green).

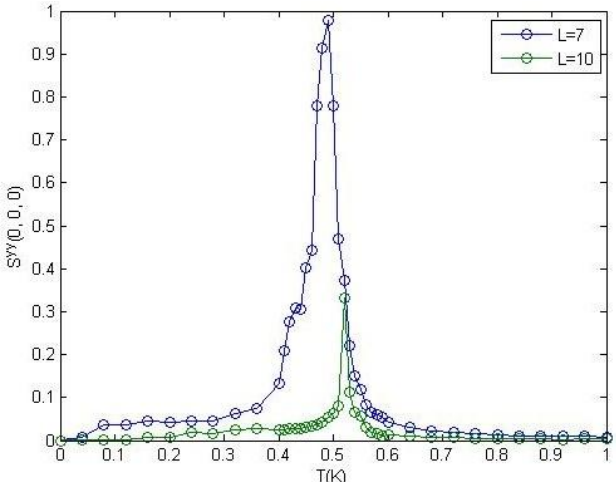

Figure 35 : S^{yy}(0,0,0) per spin as a function of the temperature for L=7 (blue) and L=10 (green).

In Fig. 35, $S^{yy}(0,0,0)$ measures the moments *y* component correlations which peaks at T_N, suggesting T_N=*0.49K* for L=7 and T_N=*0.52K* for L=10. Towards the transition the moments fluctuate more and more around their initial alignment (along the x axis) while still being correlated until the temperature completely kills the correlations. This effect is not taken into account in the mean field theory, which completely ignores local fluctuations and therefore does not give an accurate description of the system at temperatures around T_N.

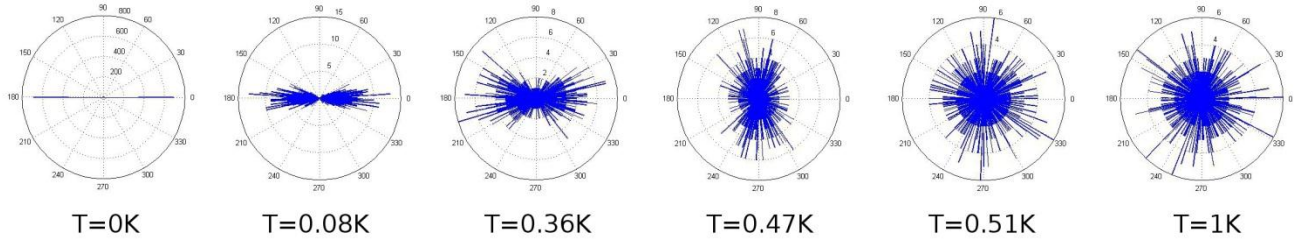

Figure 36 : Angular distribution of the moments in the (*x*,*y*) plane at different temperatures for L=7. Angles are measured from the x axis (0 or 180°).

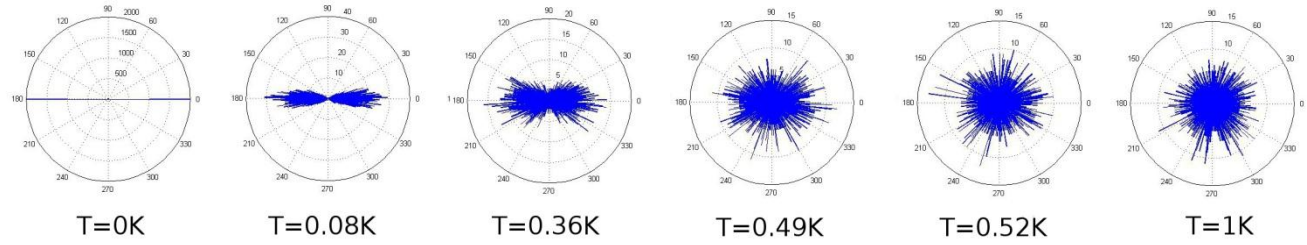

Figure 37 : Angular distribution of the moments in the (*x*,*y*) plane at different temperatures for L=10. Angles are measured from the x axis (0 or 180°).

For L=7, at 0.47K the moments seem to align on the y axis, therefore increasing $S^{yy}(0,0,0)$. This does not happen for L=10, or at least it is very less pronounced, suggesting once again finite size effects. Note that $S^{yy}(0,0,0)$ is three time smaller for L=10 than for L=7, which is consistent with the observation made on Fig. 26.

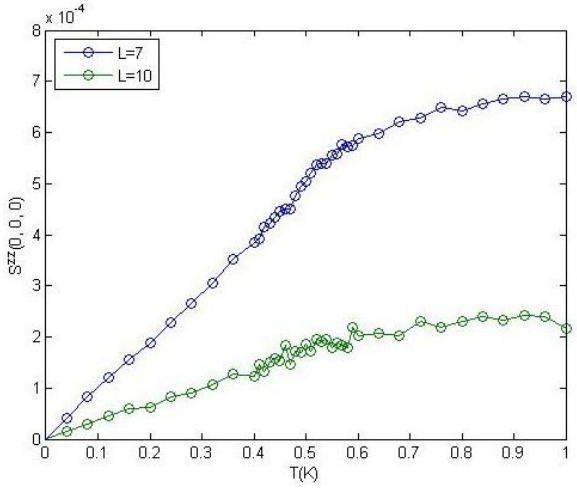

Figure 38 : $S^{zz}(0,0,0)$ per spin as a function of the temperature for L=7 (blue) and L=10 (green).

$S^{zz}(0,0,0)$ grows linearly as a function of the temperature with two different slopes before and after the transition. It is also a hundred times smaller than $S^{yy}(0,0,0)$ because of the (*x*,*y*) planar anisotropy.

One can also look at $S^{\alpha\beta}(\Delta Q,0,0)$ and $S^{\alpha\beta}(0,\Delta Q,0)$.

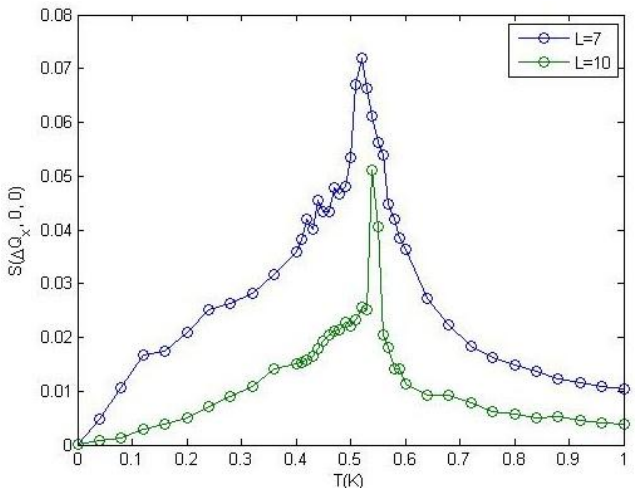

Figure 40 : $S(\Delta Q,0,0)$ per spin as a function of the temperature for L=7 (blue) and L=10 (green).

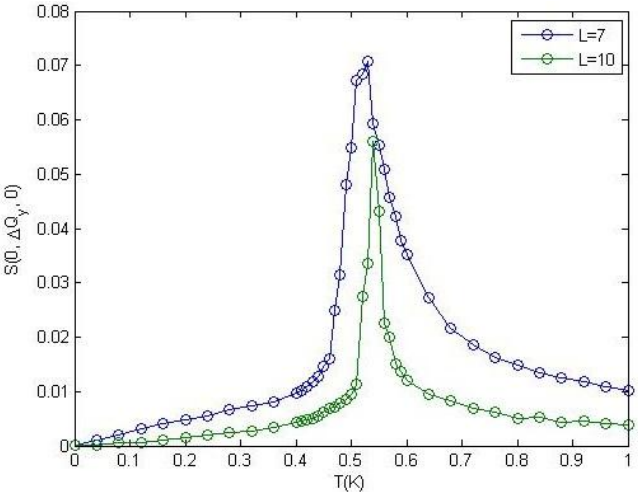

Figure 39 : $S(0,\Delta Q,0)$ per spin as a function of the temperature for L=7 (blue) and L=10 (green).

As expected, the peaks are sharper for L=10 because of the better Q resolution and they are also smaller than for L=7, just like $S^{yy}(0,0,0)$. The temperatures at which the peaks occur are slightly shifted to higher values, that is 0.52K and 0.53K for L=7, and 0.54K for

L=10. In the ordered phase, $S(\Delta Q, 0,0)$ grows faster than $S(0, \Delta Q, 0)$, but they decrease almost exactly in the same way in the disordered phase.
From this data, one can compute the critical exponents α, β and γ with

$$C = A|t|^{-\alpha} + B \tag{52}$$

$$J_{xy} = A'|t|^{\beta} + B' \tag{53}$$

$$\chi = A''|t|^{-\gamma} + B'' \tag{54}$$

Where *t* is the reduced temperature

$$t = 1 - \frac{T}{T_N} \tag{55}$$

Experimentally, it has been found that the classical phase transition features 2D XY/h_4 critical exponents $\alpha = -0.28 \pm 0.04$, $\beta = 0.15 \pm 0.02$, $\delta = 15.2$ and $\eta = 0.26$.
Critical exponents fall into universality classes and obey the following scaling relations:

$$\nu d = 2 - \alpha = 2\beta + \gamma = \beta(\delta + 1) = \gamma\frac{\delta + 1}{\delta - 1} \tag{56}$$

$$2 - \eta = \frac{\gamma}{\nu} = d\frac{\delta - 1}{\delta + 1} \tag{57}$$

Where ν the critical exponent associated with the correlation length ($\xi \propto |t|^{-\nu}$) and *d* is the dimension of the system. Using $\gamma = 2 - \alpha - 2\beta$ or $\gamma = \beta(\delta - 1)$ from (56), one should expect to find $\gamma = 1.98 \pm 0.08$ or $\gamma = 2.13 \pm 0.3$ (respectively).
For example, if one plots $\log(J_{xy}^{MC10})$ as a function of $\log(t)$ from the staggered magnetization in the ordered phase for L=10 of Fig.26, $\log(C_V)$ as a function of $\log(t)$ from the specific heat in the ordered phase for L=7 of Fig.30 and $\log(\chi)$ as a function of $\log(t)$ from the magnetic susceptibility in the disordered phase for L=7 of Fig.32:

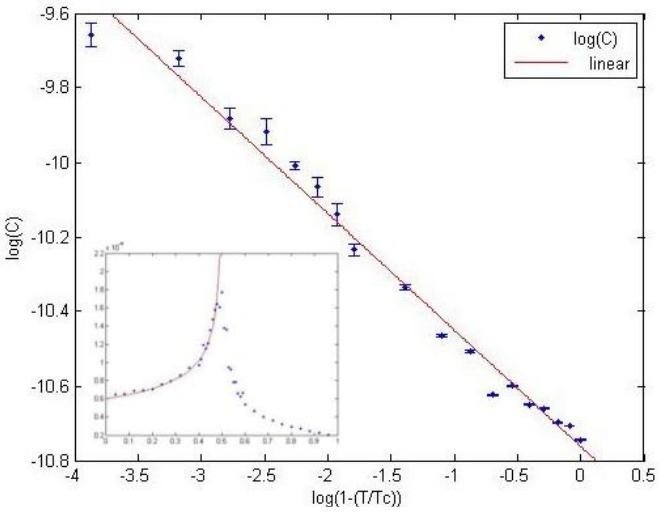

Figure 42 : Linear fitting of the α exponent from C_v for L=7 in the ordered phase.

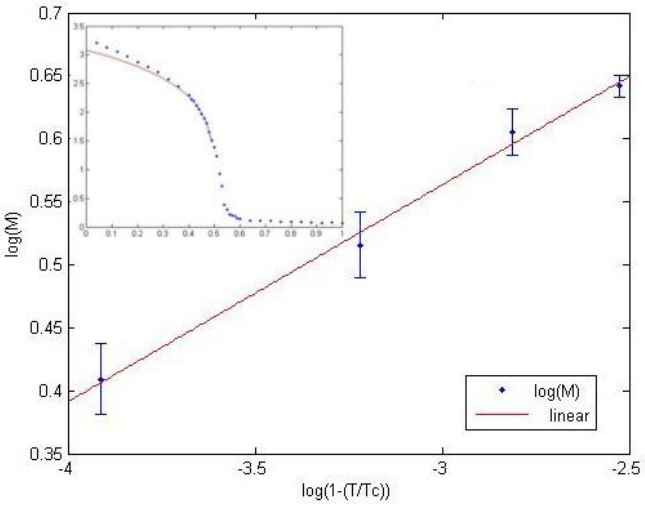

Figure 41 : Linear fitting of the β exponent for T_N=0.5K. Only the points close to the phase transition are considered.

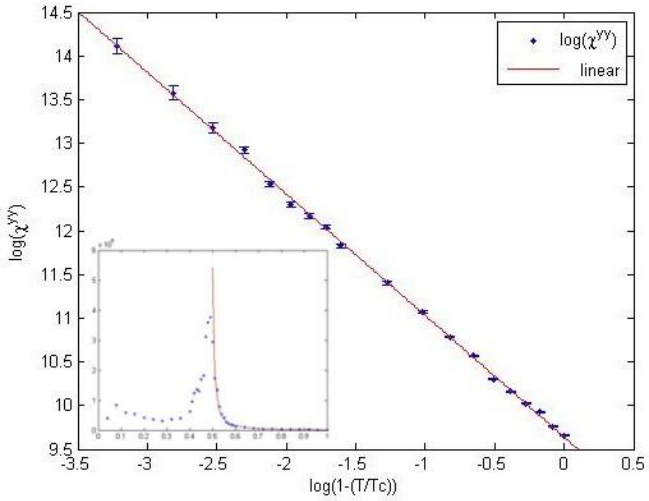

Figure 43 : Linear fitting of the γ exponent from χ^{yy} for L=7 in the disordered phase.

Using a linear fitting, one finds $\alpha = 0.33$, $\beta = 0.17$ and $\gamma = 1.5$ which is very close to what we expected.

But the critical exponents' values highly depend on the value of T_N, which is found to be between 0.48K and 0.52K, depending on the system size, on the measured quantity and the way it is computed.

	α		α_{FDT}		β		γ	
	L=7	**L=10**	**L=7**	**L=10**	**L=7**	**L=10**	**L=7**	**L=10**
T_N=0.48K	0.26	0.23	0.26	0.28	0.12	0.10	1.67	2.79
T_N=0.49K	0.29	0.25	0.28	0.29	0.15	0.13	1.50	2.54
T_N=0.50K	0.33	0.32	0.30	0.29	0.19	0.17	1.39	1.99
T_N=0.51K	0.35	0.39	0.31	0.35	0.25	0.20	1.25	2.08
T_N=0.52K	0.38	0.43	0.35	0.39	0.37	0.24	1.14	1.99

Table 1 : Values of α, β and γ depending on T_N

In Table 1, α is computed from the specific heat of Fig. 30, α_{FDT} from the specific heat of Fig. 31, β from the staggered magnetization J_{xy}^{MC}, and γ from the magnetic susceptibility of Fig. 32. Fitting γ from the magnetic susceptibility computed with the fluctuation-dissipation theorem gives $\gamma \sim 10^{-2}$ for all T_N. The highlighted cells correspond to the exponent computed with the T_N obtained from the considered quantity (i.e., χ^{yy} exhibits a peak at 0.49K for L=7 and 0.52K for L=10). For $T_N \in [0.48, 0.5]$ the fitted theoretical values of α and α_{FDT} are consistent with the experimentally measured values. As for β, the Néel temperatures yielding the smallest residuals after the linear fitting are T_N=*0.49K* and T_N=*0.5K*. For these critical temperatures the theoretical β is also consistent with a 2D XY/h_4 universality class. The γ exponent is the most difficult to fit and its value varies a lot depending on the size of the system and on T_N. Although for L=10 and $T_N \in [0.5, 0.52]$ it corresponds to the expected value calculated from the scaling relations and the other experimentally determined exponents.

Overall, for L=10 systems, which should yield more accurate exponents, α, β and γ fall in the 2D XY/h_4 universality class for T_N=*0.49K* and T_N=*0.5K*.

CONCLUSION

Much of this work consisted in developing a reduced but tangible model of $LiREF_4$ compounds (RE = Er or Ho), checking its validity with mean field calculations, and implementing it in a simulated annealing algorithm.

The preliminary simulations performed using the mean field theory on $LiErF_4$ yield a qualitatively correct behavior but an overestimated Néel temperature of 767mK because it neglects fluctuations. It also allowed revealing the emergence of a second antiferromagnetic ordering at high fields in $LiErF_4$. Experimental measurements of this new phase will help to calculate the critical exponents of classical and quantum phase transitions in order to compare their universality classes with those of the low field phase.

A functional effective model, very faithful to the full model has been built for $LiErF_4$, but needs to be improved to make it suitable to Ho^{3+} ions because it doesn't account for the hyperfine interaction nor for the singular anisotropy effect on the ground state doublet. Holmium ions can still be incorporated in the lattice by considering them to be pure Ising spins, that is only ± 1. This approximation, while being very simplistic and a little bit unrealistic, has nevertheless always been used in theoretical studies of $LiHoF_4$ so far.

Despite the implementation in C and the use of vectorized MATLAB programming which allowed to divide the computational time by a factor 100, the Monte Carlo calculations are still onerous and need more than two weeks to lead L=10 systems to equilibrium on a computer cluster. Moreover, the results are highly dependent of the system size, indicating that the thermodynamic limit may not be reached yet and that simulations of larger systems should be undertaken. Also, the uncertainty about the quality of the data for L=10 does not allow to extract exact results in a trustworthy way.

But with a reduced Néel temperature lying between 0.48K and 0.52K, and theoretical critical exponents that are consistent with the experimentally measured ones, the classical Monte Carlo study of $LiErF_4$ provides results much closer to reality than the mean-field simulations. The good concordance of the critical exponents indicate that the effective model correctly renders the 2D scaling. The shape of the specific heat, whether it is computed by differentiating the energy or from the fluctuation-dissipation theorem, is also remarkably very close to the one determined experimentally. The simulated annealing code achieved during this master thesis therefore seems very promising for the study of the diluted compound $LiEr_xY_{1-x}F_4$ and could perhaps even reveal the existence of a spin glass phase in $LiHo_{0.167}Y_{0.833}F_4$.

As for $LiHo_xEr_{1-x}F_4$, we know that for x between 0.5 and 0.8 there is a "crossover" area where the system goes from an ordered phase to a spin glass. A numerical simulation can be conducted with this simulated annealing code to determine the behavior of this system around its critical point.

BIBLIOGRAPHY

[1] A. Biltmo and P. Henelius, Phase diagram of the dilute magnet $LiHo_xY_{1-x}F_4$, *Phys. Rev. B 76*(5), 054423 (2007).

[2] D. Bitko, T. F. Rosenbaum, and G. Aeppli, Quantum critical behavior for a model magnet, *Phys. Rev. Lett. 77*, Vol. 5, pp940-943 (1996).

[3] R. M. Brannon, A review of useful theorems involving proper orthogonal matrices referenced to three dimensional physical space (www.mech.utah.edu/brannon/public/rotation.pdf) (2002).

[4] J. Brooke, D. Bitko, T. F. Rosenbaum, and G. Aeppli, Quantum annealing of a disordered magnet, *Science 284*, p779 (1999).

[5] J. Brooke, T. F. Rosenbaum, and G. Aeppli, Tunable quantum tunnelling of magnetic domain walls, *Nature 413*, p610 (2001).

[6] V. Cannella and J. A. Mydosh, Magnetic Ordering in Gold-Iron Alloys, *Phys. Rev. B 6*, p4220 (1972).

[7] P. B. Chakraborty, P. Henelius, H. Kjønsberg, A. W. Sandvik, and S. M. Girvin , Theory of the magnetic phase diagram of lihof4 , *Phys. Rev. B 70*(14), 144411 (Oct 2004).

[8] S. Ghosh, R. Parthasarathy, T. F. Rosenbaum, and G. Aeppli, *Science 296*, p2195 (2002).

[9] S. Ghosh, T. Rosenbaum, G. Aeppli, and S. Coppersmith, Entangled quantum state of magnetic dipoles, *Nature 425*, p48 (2003).

[10] C. L. Henley, Selection by quantum fluctuations of dipolar order in a diamond lattice (commentaire), *Phys. Rev. Lett. 73*, p2788 (1994).

[11] A.J.Hertz, *Phys. Rev. B 14*, p1165 (1976).

[12] *International Tables for Crystallography* (Kluwer, Dordrecht, 2002), Vol. A: Space-group symmetry.

[13] J. Jensen and A. R. Mackintosh, Rare Earth Magnetism, Oxford Univ. Press (1991).

[14] P. E. Jönsson, R. Mathieu, W. Wernsdorfer, A. Tkachuk, and B.Barbara, *Phys. Rev. Lett. 98*, p256403 (2007).

[15] H. Kjønsberg and S. M. Girvin, The classical phase transition in $LiHoF_4$: Results from mean field theory and Monte Carlo simulations, *American Institute of Physics Conference Series*, volume 535, pp323–331, September 2000.

[16] C. Kraemer et al., Dipolar antiferromagnetism and quantum criticality in LiErF4, *Science 336*, pp1416-1419 (2012).

[17] C. Kraemer, Quantum phase transition in a magnetic model system, *PhD thesis*, Laboratory for Quantum Magnetism (LQM-EPFL) (2009).

[18] J. M. Luttinger and L. Tisza, Theory of Dipole Interaction in Crystals, *Phys. Rev. 70*, p954 (1946).

[19] S. K. Misra and J. Felsteiner, Low-temperature ordered states of lithium rare-earth tetrafluorides, *Phys. Rev. B 15*, p4309 (1977).

[20] J. Piatek, *Thèse de Master*, Laboratory for Quantum Magnetism (LQM-EPFL) (2009).

[21] D. H. Reich, B. Ellman, J. Yang, T. F. Rosenbaum, G. Aeppli, and D. P. Belanger, Dipolar magnets and glasses: Neutron-scattering, dynamical, and calorimetric studies of randomly distributed Ising spins, *Phys. Rev. B 42*, pp4631–4644 (Sep 1990).

[22] H. M. Ronnow et al., Quantum phase transition of a magnet in a spin bath, *Science 308*, p389 (2005).

[23] M. Schechter and N. Laflorencie, Quantum spin glass and the dipolar interaction, *Phys. Rev. Lett. 97*, 137204 (2006).

[24] D. Silevitch et al., A ferromagnet in a continuously tunable random field, *Nature 448*, p567 (2007).

[25] K. W. H. Stevens, in: *Magnetism Vol. 1* (Academic Press, New York), Edited by G. T. Rado and H. Suhl, pp1-23 (1973).

[26] K. W. H. Stevens, Matrix elements and operator equivalents connected with the magnetic properties of rare earth ions, *Proceedings of the Physical Society A*, 65, p209 (1952).

[27] S. M. A. Tabei et al., Perturbative Quantum Monte Carlo Study of LiHoF4 in a Transverse Magnetic Field, *Phys. Rev. Lett. 97*, p237203 (2006).

[28] Ka-Ming Tam and Michel J. P. Gingras, Spin glass transition at nonzero temperature in a disordered dipolar system: The case of $LiHo_xY_{1-x}F_4$, *Phys. Rev. Lett. 103*, 087202 (2008).

[29] A. Tkachuk and V. Shumilin, *European Conference on Lasers and Electro-Optics* (CLEO), p137 (28 Aug-2 Sep 1994).

[30] W. Wu, D. Bitko, T. F. Rosenbaum, and G. Aeppli, *Phys. Rev. Lett. 71*, p1919 (1993).

APPENDIX

1. Crystallographic details $LiREF_4$

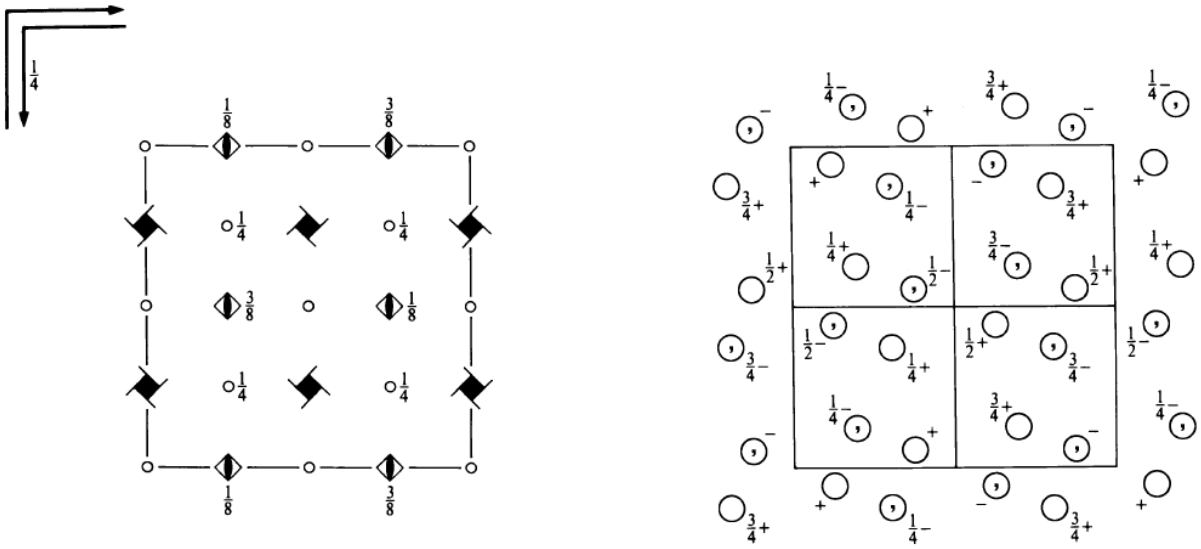

Figure 44 : *I4₁/a* space group symmetries according to *International Tables for Crystallography* [12] (n°88, origin choice 2).

The positions of the ions within the $LiREF_4$ cell unit are given in Table 1. RE^{3+} ions occupy sites with the Wyckoff letter *b*, Li^{3+} occupy sites *a* and F^- the sites f.
Because of the asymmetry, the positions of the fluoride ions must meet the following conditions:

$$0 \le x \le \frac{1}{4} \qquad 0 \le y \le \frac{1}{4} \qquad 0 \le z \le 1$$

Multiplicity			Coordinates
Wyckoff letter			
Site Symmetry			$(0,0,0)+$ $(\frac{1}{2},\frac{1}{2},\frac{1}{2})+$
16	f	1	(1) x,y,z (2) $\bar{x}+\frac{1}{2},\bar{y},z+\frac{1}{2}$ (3) $\bar{y}+\frac{3}{4},x+\frac{1}{4},z+\frac{1}{4}$ (4) $y+\frac{3}{4},\bar{x}+\frac{3}{4},z+\frac{3}{4}$
			(5) $\bar{x},\bar{y},\bar{z}$ (6) $x+\frac{1}{2},y,\bar{z}+\frac{1}{2}$ (7) $y+\frac{3}{4},\bar{x}+\frac{1}{4},\bar{z}+\frac{1}{4}$ (8) $\bar{y}+\frac{3}{4},x+\frac{3}{4},\bar{z}+\frac{3}{4}$
4	b	$\bar{4}$	$0,\frac{1}{4},\frac{5}{8}$ $\frac{1}{2},\frac{1}{4},\frac{7}{8}$
4	a	$\bar{4}$	$0,\frac{1}{4},\frac{1}{8}$ $\frac{1}{2},\frac{1}{4},\frac{3}{8}$

Table 2 : Crystallographic positions within the unit cell in the space group *I4₁/a* according to [12] (n°88, origin choice 2).

	c [Å]	a [Å]
$LiTbF_4$	10.873	5.181
$LiYbF_4$	10.59	5.132
$LiTmF_4$	10.64	5.15
$LiDyF_4$	10.83	5.189
$LiHoF_4$	10.75	5.175
$LiYF_4$	10.74	5.175
$LiErF_4$	10.70	5.162

Table 3: Lattice parameters of a few $LiREF_4$ compounds [17].

2. Crystal field parameters and Stevens operators

$$O_2^0 = 3J_z^2 - X$$
$$O_4^0 = 35J_z^4 - (30X - 25)J_z^2 + 3X^2 - 6X$$
$$O_4^4 = \frac{1}{2}(J_+^4 + J_-^4)$$
$$O_6^0 = 231J_z^6 - (315X - 735)J_z^4 + (105X^2 - 525X + 294)J_z^2 - 5X^3 + 40X^2 - 60X$$
$$O_6^4(c) = \frac{1}{4}[(11J_z^2 - X - 38)(J_+^4 + J_-^4) + (J_+^4 + J_-^4)(11J_z^2 - X - 38)]$$
$$O_6^4(s) = \frac{1}{4i}[(11J_z^2 - X - 38)(J_+^4 - J_-^4) + (J_+^4 - J_-^4)(11J_z^2 - X - 38)]$$

Table 4 : Stevens operators, with X=J(J+1)

$10^3B_2^0$	$10^3B_4^0$	$10^3B_4^4(c)$	$10^3B_4^4(s)$	$10^6B_6^0(c)$	$10^6B_6^4(c)$	$10^6B_6^4(s)$
63.0±5.9	-0.55±0.03	-5.54±0.07	0.47±0.01	-0.006±0.006	-108.2±1.2	-14.6±0.5

Table 5 : $LiErF_4$ crystal field parameters (in meV) [17].

$10^3B_2^0$	$10^3B_4^0$	$10^3B_4^4(c)$	$10^6B_6^0(c)$	$10^6B_6^4(c)$	$10^6B_6^4(s)$
-63.2±4.8	0.318±0.016	3.42±0.04	0.55±0.01	60.1±0.1	18.9±0.1

Table 6 : $LiHoF_4$ crystal field parameters (in meV) [17].

3. Phase transitions of some $LiREF_4$ compounds

- $LiTmF_4$

The exchange coupling and the hyperfine interaction are ignored here. Whatever the initial configuration of the moments is, and regardless of the direction along which the external magnetic field is applied, the mean field algorithm indicates that there is no magnetic order at zero external field:

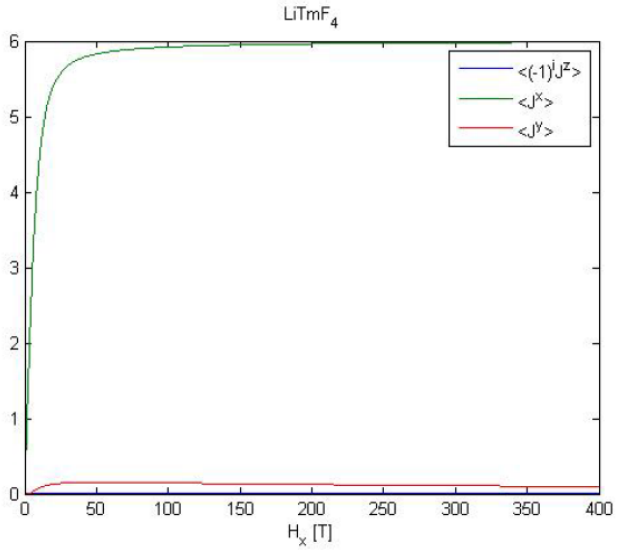

Figure 46 : Quantum phase transition of $LiTmF_4$ when the field is applied along the x axis (in green the magnetization along x, in red the magnetization along y).

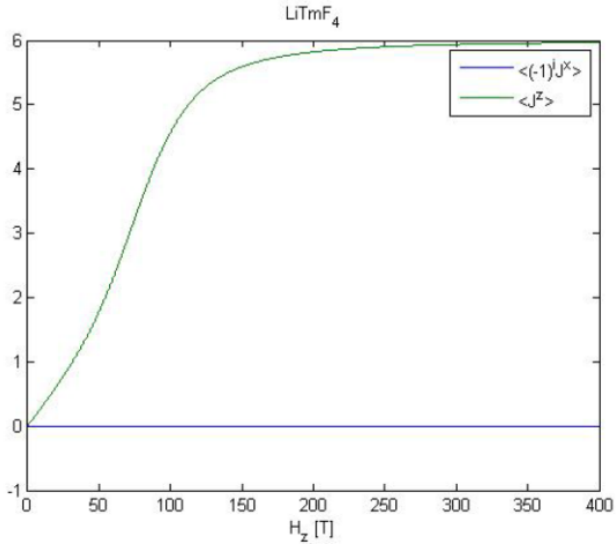

Figure 45 : Quantum phase transition of $LiTmF_4$ when the field is applied along the z axis (in blue the magnetization along x, in green the magnetization along z).

This can be explained by the fact that the ground state is not degenerated at zero field.

- $LiYbF_4$

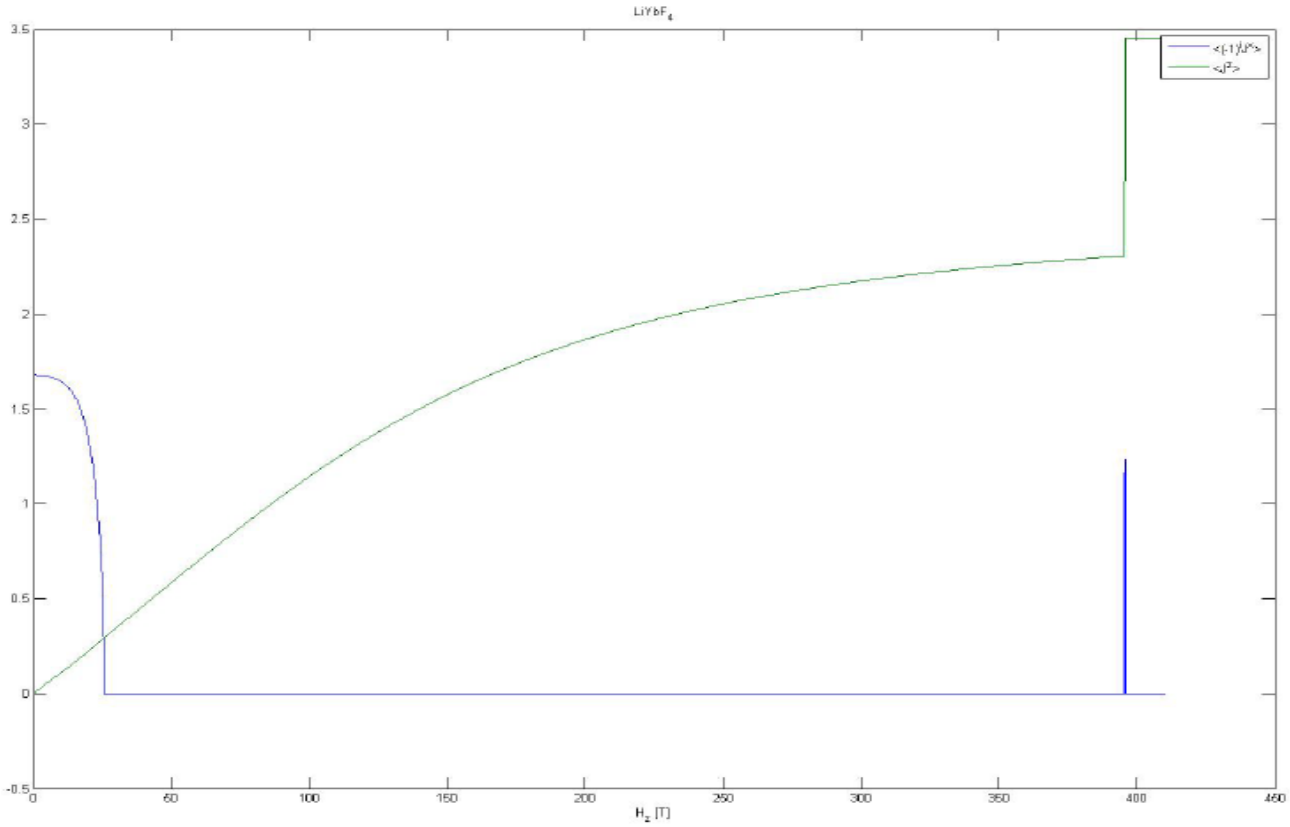

Figure 47 : Quantum phase transition of LiYbF4 with a field applied along the z axis (in blue the staggered magnetization along x, in green the magnetization along z).

There is a first phase transition at 25.7T, a second one at 395.6T and a third one at 396T. The enormous value of the first critical temperature is explained by the slow splitting of the ground state doublet, which is also non-linear:

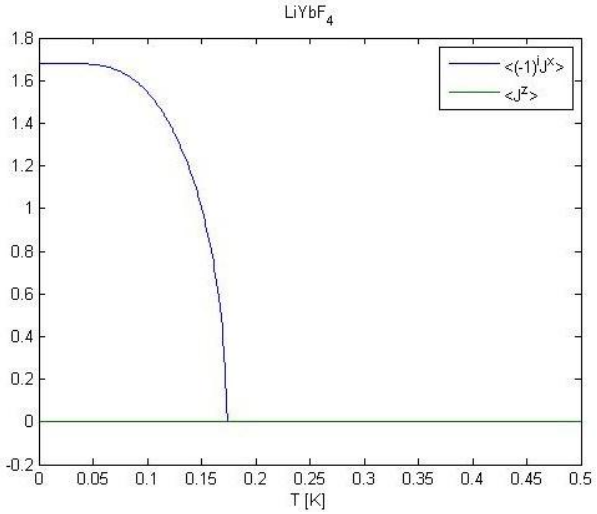

Figure 49 : Classical phase transition of LiYbF4

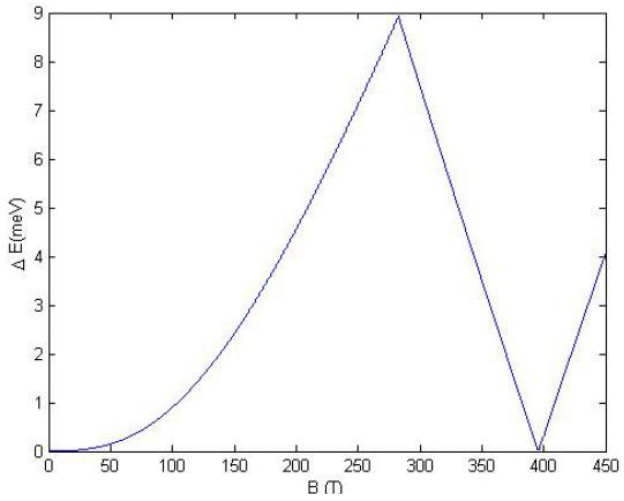

Figure 48 : Splitting of the ground state doublet of LiYbF4

- $LiGdF_4$

In the case of gadolinium the quantum number L is zero, and as the crystal field acts only on the orbital part, it has no influence on the Gd ions. We can then run the mean field calculation starting with any configuration of moments.
By starting from an antiferromagnetic configuration:

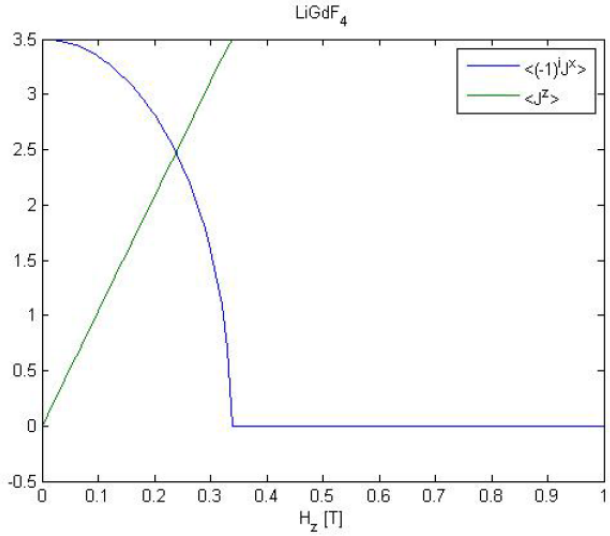

Figure 51 : Quantum phase transition of $LiGdF_4$ when the field is applied along the z axis (in blue the staggered magnetization along x, in green the magnetization along z).

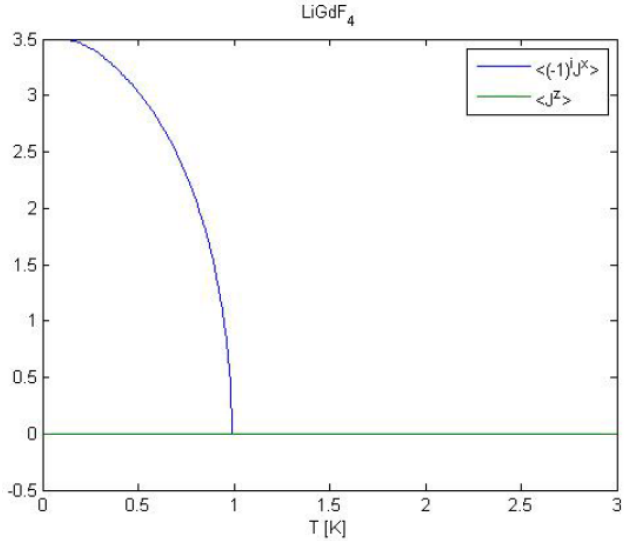

Figure 50 : Thermal phase transition of $LiGdF_4$ (in blue the staggered magnetization along x, in green the magnetization along z).

But if one starts in a ferromagnetic ordering with moments aligned along the *c* axis, the system still instantaneously settle in an antiferromagnetic order:

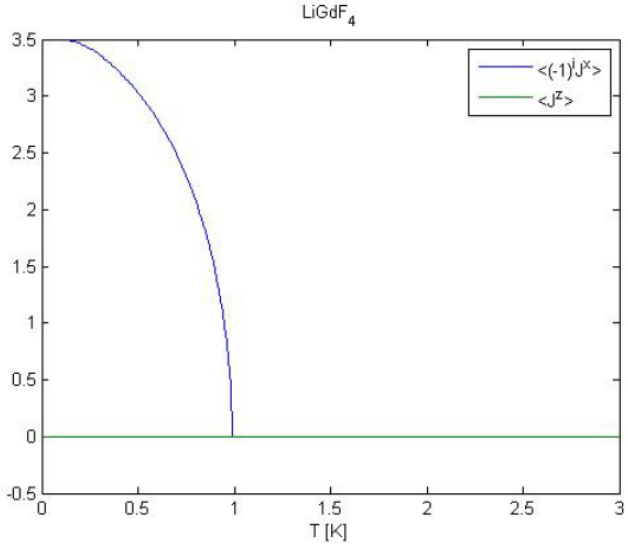

Figure 52 : Thermal phase transition of $LiGdF_4$ starting from ferromagnetic order along z (in blue the staggered magnetization along x, in green the magnetization along z).

It seems that despite the absence of crystal field, the symmetry is broken and antiferromagnetic order in the (*x, y*) plane is always favorable. Other simulations suggest that the lattice parameters play an important role in this symmetry breaking. It becomes interesting to compare the evolution of the energies of ferromagnetic (FM) and antiferromagnetic (AFM configurations) for a fixed value of the field:

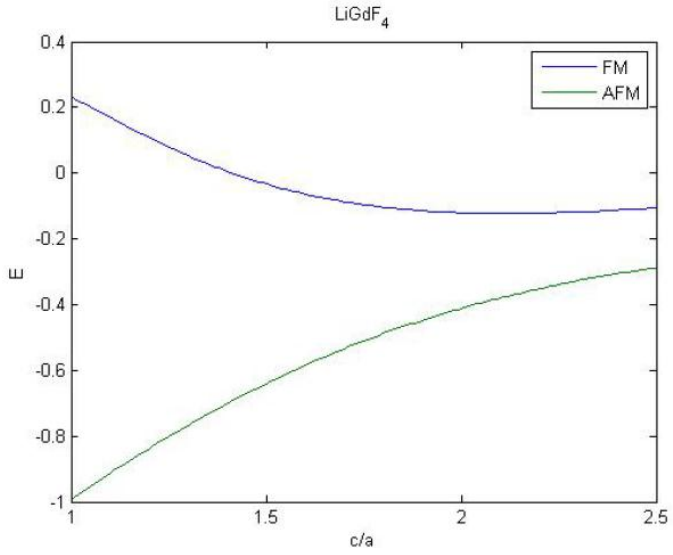

Figure 53 : Energies of the FM (blue) and AFM (green) states as a function of the lattice parameters ratio c/a at zero field.

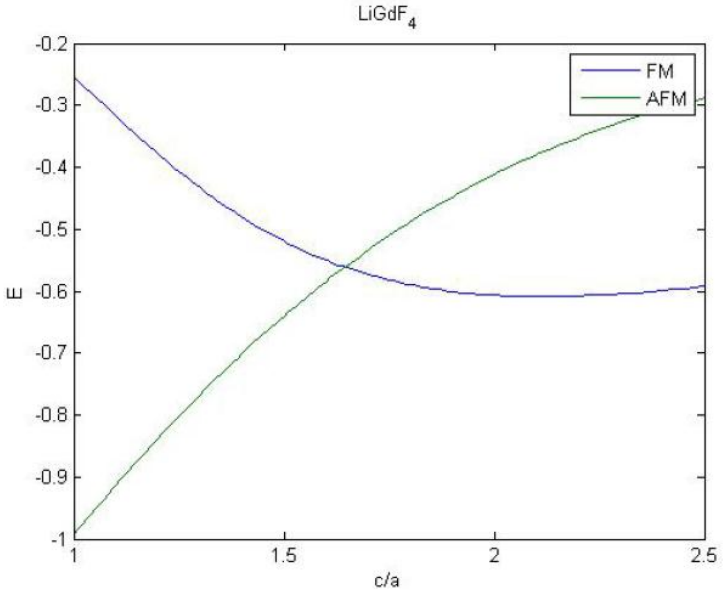

Figure 54 : Energies of the FM (blue) and AFM (green) states as a function of the lattice parameters ratio c/a at 0.3T.

The ferromagnetic order can be favorable by applying a weak external field and by expanding the sample along the c axis ($\frac{c}{a} \approx 2.1$ for the regular lattice).